Article Body Template

- **Abstract:** Mn(II) has several favorable physico-chemical characteristics and a much better toxicity profile, which makes it a viable alternative to the Gd(III)-based Magnetic Resonance Imaging (MRI) contrast agents currently used in clinics. Although many studies have been undertaken in the last ten years, this is a field of investigation still in rapid and continuous development. This review aims to critically discuss the chemical and magnetic properties of Mn(II) compounds relevant as MRI probes, both small complexes and nanosystems containing a large number of metal centers, the possible approaches for optimizing their efficiency by understanding the role of various molecular parameters that control the relaxation processes, and the most important issues related to stability and kinetic inertness.

- **Keywords:** Manganese, Magnetic Resonance Imaging, Contrast agents, Relaxometry, Chelating ligands

- **Main body of text:**

Introduction

After the initial experiments in the early ’70s, the decade of the 1980s is characterized by the advent and remarkable growth of MRI, which has evolved rapidly into one of the most powerful techniques in clinical diagnostic and biomedical research. This is due to many favourable properties, among which the following stand out: i) lack of ionizing radiation for image acquisition; ii) non-invasiveness with a high patient acceptability; iii) excellent delineation of anatomical structures; iv) superb temporal and spatial resolution (mm scale); v) possibility of application to virtually any body district.[1] The traditional imaging procedures have been combined with the use of dedicated contrast media, to help enhance the visualization of morphology and physiology. The synergistic action and the combination of technical progress with the development of new contrast agents (CAs) have been very important factors for the emergence of modern clinical radiology. In this context, MRI has not evolved along a different path and, since the advent in early ’80, this imaging modality has been improved by the use of exogenous agents to increase the signal intensity and diagnostic confidence and reduce overall cost. About one third of all routine clinical MRI procedures use intravenously introduced magnetic agents to alter image contrast.[2] Contrast agents on the market and most on those in clinical or pre-clinical trials focus upon changes of nuclear magnetic relaxation times ($T_{1,2}$). In general, the Gd(III) complexes represent the class of MRI CAs most commonly and widely used in clinical applications and in pre-clinical studies. These compounds exhibit an excellent effectiveness in catalyzing the T_1 and T_2 relaxation of the water protons in tissues where they are distributed. This choice is due to the combination of high magnetic moment and favourable properties in terms of electronic relaxation of the [Xe]4f^7 electron configuration (seven unpaired electrons in an *S* ground state). Contrast-enhanced MRI is used annually in approximately 30 million procedures with over 300 million patients having been dosed so far.[3] Gadolinium-based contrast agent are used to improve the clarity and quality of images of the body’s internal structures, which in turn helps improving the diagnostic accuracy of MRI scans. Gadolinium-based contrast agents

(GBCAs) are considered safe as MRI CAs when used at recommended dosage since the complexes are completely excreted from the body in an intact state.

However, over the last decade, new questions have arisen about the safety of gadolinium-based contrast agents. Initial concerns emerged unexpectedly but dramatically in 2006, when the use of GBCAs was associated with the development of nephrogenic systemic fibrosis (NSF), a very serious and sometimes fatal disease developed in patients with impaired renal function.[4] More recently, a growing body of data pointed to gadolinium accumulation in tissues of patients who were exposed repeatedly to GBCAs.[5] Even though no consequences of gadolinium deposition for patient health and no adverse health effects have been identified so far, there is renewed interest in the search for possible and effective alternatives to the Gd(III) complexes.

Among these, Mn(II) complexes appear to represent an obvious possibility, yet with considerable potential. The reasons are manifold and well established.[6] In fact, considering that manganese is a biogenic element, living organisms are able to manage efficiently small excess amounts of free metal ions in organs and tissues. In addition, Mn(II) chelates with d^5 high spin configuration present a high effective magnetic moment, long electronic relaxation times and quite fast exchange rates of the coordinated water molecules. These properties are associated with the efficient mechanism of interaction (electron-nuclear dipolar coupling) between the paramagnetic centre and the protons of the nearby water molecules. In spite of the favourable properties, only one Mn(II) CA has been introduced in clinical use (mangafodipir trisodium, $[Na_3[Mn(H_3DPDP)]$, TESLASCAN®).[7] This complex is hepatocyte specific and releases free Mn(II) ions, which accumulate in the liver then providing an enhanced image contrast.[8] In the last decade, studies on Mn(II) as potential MRI probes have intensified, and we have now a better understanding of the relationship between the molecular parameters of the chelates and their NMR relaxation properties in aqueous media.[9]

In this review, we want to provide the basis for understanding the behaviour of Mn(II) systems as MRI probes: relaxation mechanisms and efficiency as compared to the Gd(III) analogues; thermodynamic stability and inertness; range of chemical structures investigated; variety of multimeric and nanosized structures designed and developed. This is not intended to be an exhaustive review, since some excellent ones are available,[6, 10, 11] but rather we will discuss critically only selected examples that help to illustrate the concepts and show the potential and limitations of Mn(II)-based MRI contrast agents.

Background and Theory

Equations for paramagnetic relaxation adapted to Mn(II)

The relaxivity (r_{1p}) of a paramagnetic probe is a parameter that measures its efficiency as a contrast agent and it is defined as the gain in the relaxation rate of water proton nuclei induced by a 1 mM concentration of the paramagnetic agent. The observed longitudinal proton relaxation rate (R_1^{obs}) is the result of a diamagnetic (R_1^d) and a paramagnetic (R_1^p) contribution, with the latter being proportional to the concentration of paramagnetic agent:[12]

$$R_1^{obs} = R_1^d + R_1^p = R_1^d + r_{1p}[\mathrm{Mn(II)}] \quad (1)$$

Thus, a plot of R_1^{obs} versus the concentration of the paramagnetic ion should give a straight line whose slope corresponds to the proton relaxivity of the agent r_{1p}, generally expressed in s^{-1} mM^{-1} units. The observed relaxivity can be divided into inner- ($r_{1p,is}$) and outer-sphere ($r_{1p,os}$) terms:[13]

$$r_{1p} = r_{1p,is} + r_{1p,os} \quad (2)$$

The outer-sphere contribution describes a long range dipolar coupling between the electron spin of the paramagnetic ion and the nuclear spin of water protons diffusing in the surroundings of the paramagnetic center. The outer-sphere contribution is generally described by Freed's model according to the following expressions:[14]

$$r_{1p,OS} = \frac{32N_A\pi}{405}\left(\frac{\mu_0}{4\pi}\right)^2 \frac{\hbar^2\gamma_S{}^2\gamma_I{}^2}{a_{MnH}D_{MnH}} S(S+1)[3J_{OS}(\omega_I;T_{1e}) + 7J_{OS}(\omega_I;T_{2e})] \quad (3)$$

$$J_{OS}(\omega_I;T_{je}) = Re\left[\frac{1+\frac{1}{4}\left(i\omega\tau_{MnH}+\frac{\tau_{MnH}}{T_{je}}\right)^{1/2}}{1+\left(i\omega\tau_{MnH}+\frac{\tau_{MnH}}{T_{je}}\right)^{1/2}+\frac{4}{9}\left(i\omega\tau_{MnH}+\frac{\tau_{MnH}}{T_{je}}\right)+\frac{1}{9}\left(i\omega\tau_{MnH}+\frac{\tau_{MnH}}{T_{je}}\right)^{3/2}}\right] \quad (4)$$

$$\tau_{MnH} = \frac{a_{MnH}{}^2}{D_{MnH}} \quad (5)$$

In Eqs (3)-(5) N_A is the Avogadro constant, a_{MnH} is the distance of closest approach of an outer-sphere water molecule to the Mn center, T_{1e} and T_{2e} are the longitudinal and transverse relaxation times of the electron spin, S is the electron spin, γ_I and γ_S are the nuclear and electron gyromagnetic ratios, and D_{MnH} is the relative translational diffusion coefficient, calculated as the sum of the self-diffusion coefficients of the Mn complex and water molecules. The longitudinal and transverse electronic relaxation rates are generally approximated by Eqs (6)-(7), where τ_V describes the correlation time associated with the modulation of the zero-field-splitting (ZFS) interaction, Δ^2 is the mean square ZFS energy and ω_S is the electron Larmor frequency.[15]

$$\frac{1}{T_{2e}} = \frac{1}{25}\Delta^2\tau_v\{4S(S+1)-3\}\left(\frac{1}{1+\omega_S{}^2\tau_v{}^2}+\frac{4}{1+4\omega_S{}^2\tau_v{}^2}\right) \quad (6)$$

$$\frac{1}{T_{2e}} = \frac{1}{50}\Delta^2\tau_v\{4S(S+1)-3\}\left(3+\frac{5}{1+\omega_S{}^2\tau_v{}^2}+\frac{2}{1+4\omega_S{}^2\tau_v{}^2}\right) \quad (7)$$

The inner-sphere contribution to relaxivity, $r_{1p,is}$, is directly proportional to the number of water molecules coordinated to the metal ion, q:

$$r_{1p,is} = \frac{1}{1000}\times\frac{q}{55.55}\times\frac{1}{T_{1m}^H+\tau_m} \quad (8)$$

In Eq (8) τ_m is the mean residence time of a water molecule in the inner coordination sphere of the metal ion and $1/T_{1m}^H$ is the relaxation rate of inner sphere protons, which for Mn(II) complexes may arise from dipole-dipole (DD) and scalar (SC) mechanisms according to:[16-17]

$$\left(\frac{1}{T_{1m}^H}\right)^{DD} = \frac{2}{15}\left(\frac{\mu_0}{4\pi}\right)^2\frac{\gamma_I{}^2g^2\mu_B{}^2}{r_{MnH}{}^6}S(S+1)\left(\frac{3\tau_{d1}}{1+\omega_I{}^2\tau_{d1}{}^2}+\frac{7\tau_{d2}}{1+4\omega_S{}^2\tau_{d2}{}^2}\right) \quad (9)$$

$$\left(\frac{1}{T_{1m}^H}\right)^{SC} = \frac{2S(S+1)}{3}\left(\frac{A}{\hbar}\right)^2\left(\frac{\tau_{e2}}{1+\omega_S{}^2\tau_{e2}{}^2}\right) \quad (10)$$

$$\frac{1}{\tau_{di}} = \frac{1}{\tau_R}+\frac{1}{\tau_m}+\frac{1}{T_{ie}}, \text{with } i = 1,2 \quad (11)$$

$$\frac{1}{\tau_{e2}} = \frac{1}{\tau_m}+\frac{1}{T_{ie}} \quad (12)$$

In these equations g is the electron g factor, μ_B is the Bohr magneton, ω_I is the nuclear Larmor frequency, r_{MnH} is the distance between the electron and nuclear spins, $A/\hbar$ is the scalar coupling constant and τ_R is the rotational correlation time.

Mn(II) vs Gd(III) contrast agents

Outer-sphere relaxation

The outer-sphere contribution to relaxivity is proportional to $S(S+1)$, as shown in Eq 3. A Mn(II) complex with a high-spin configuration is characterized by $S(S+1) = 8.75$, while the $4f^7$ configuration of Gd(III) yields $S(S+1) = 15.75$. Thus, the $r_{1p,os}$ values of Mn(II) complexes are expected to be 1.8 lower than those of Gd(III) analogues if the distance of closest approach, the diffusion coefficient and electronic relaxation times take comparable values. A comparison of the nuclear magnetic relaxation dispersion (NMRD) profiles of $[Mn(DO3A)]^-$ and $[Gd(Me2DO2PA)]^+$ complexes,[18-19] which lack inner-sphere water molecules, evidences this effect (Figure 1). The relaxivity observed for $[Gd(Me2DO2PA)]^+$ is higher than that of $[Mn(DO3A)]^-$ over the whole range of proton Larmor frequencies, as would be expected. The analysis of the data provided similar parameters for the relaxation of the electron spin ($\Delta^2 = 7.4\times10^{19}$ s^{-2} and $\tau_v = 18.1$ ps for $[Mn(DO3A)]^-$, and $\Delta^2 = 12\times10^{19}$ s^{-2} and $\tau_v = 14.9$ ps for $[Gd(Me2DO2PA)]^+$). The values of the diffusion coefficient are also similar ($D_{MnH} = 23.5\times10^{-10}$ m^{2}s^{-1} and $D_{GdH} = 21.7\times10^{-10}$ m^{2}s^{-1}), as water diffuses much faster than the complexes, so that the relative diffusion coefficient should be close to the self-diffusion coefficient of water.

Inner-sphere relaxation

The inner-sphere contribution to relaxivity in Gd(III) complexes is dominated by the dipole-dipole mechanism, while for some Mn(II) complexes both the dipole-dipole and scalar mechanisms provide a significant contribution to the overall relaxivity. A typical example is the octahedral aquated Mn(II) ion, which presents a NMRD profile showing two dispersions (Figure 2).[20] The first dispersion, which is observed in the 2-20 MHz range, is characteristic of both Mn(II) and Gd(III) complexes.[21] However, the $[Mn(H_2O)_6]^{2+}$ ion gives a second dispersion at lower field (0.02-0.5 MHz) that is absent in the case of Gd(III), and indicates the presence of a scalar contribution to relaxivity. The analysis of the data provided a scalar hyperfine coupling constant of $A/\hbar = 5.43\times10^6$ rad s^{-1}. Nevertheless, the scalar contribution is rarely observed for Mn(II) complexes other than the aquated ion. This can be understood by calculating the scalar contribution to r_{1p} with the use of Eq (10) as a function of τ_m and $1/T_{2e}$ (Figure 3). This simulation shows that the scalar contribution increases for long τ_m values (low $k_{ex} = 1/\tau_m$) and slow electronic relaxation. The $[Mn(H_2O)_6]^{2+}$ ion presents a rather long τ_m of 35 ns, while Mn(II) complexes other than the aqua ion generally present faster water exchange rates (see below). On the other hand, the high symmetry of the octahedral $[Mn(H_2O)_6]^{2+}$ complex results in a small zero-field splitting energy, resulting in a very slow relaxation of the electron spin. Thus, it is not surprising that Mn(II) complexes other than $[Mn(H_2O)_6]^{2+}$ often present negligible scalar contribution to the observed relaxivity.

The relaxivity of the aquated Gd(III) ion is higher than that of $[Mn(H_2O)_6]^{2+}$ at proton Larmor Frequencies > ~1 MHz (Figure 2). This can be rationalized by inspecting Eqs (8) and (9). First, the inner-sphere contribution to relaxivity is

directly proportional to the number of coordinated water molecules *q*, which favours a higher relaxivity of the octacoordinated Gd(III) ion. Second, the slightly longer τ_R value of $[Gd(H_2O)_8]^{3+}$ also favours a higher relaxivity at high fields (>~10 MHz). These two effects are obviously not balanced by the shorter r_{MnH} distance (typically ~2.8 Å) compared to the r_{GdH} value (3.1 ± 0.1 Å),[22] in spite of the inverse sixth power dependence of the dipolar relaxation rate with the distance between the nuclear and electron spins. Table 1 presents a comparison of the relevant parameters governing the relaxivity of the $[Mn(H_2O)_6]^{2+}$ and $[Gd(H_2O)_8]^{3+}$ systems, which were obtained by combined analysis of ^{1}H NMRD and ^{17}O NMR data.

Figure 4 presents the NMRD profiles obtained for two typical complexes with polyaminocarboxylate ligands containing one coordinated water molecule, $[Mn(EDTA)]^{2-}$ and $[Gd(DTPA)]^{2-}$. The ^{1}H NMRD profiles of the two complexes present very similar shapes, showing a single dispersion in the range 2-20 MHz. The relaxivities of the Gd(III) complex are higher over the whole range of magnetic field strengths, which can be attributed to the 1.8 factor arising from the ratios of the $S(S+1)$ term and the longer τ_R value of the Gd(III) derivative. This effect is in part compensated by the shorter distance between the nuclear and electron spin in the Mn(II) complex, which is associated to the shorter Mn-O_{water} distance compared to the Gd-O_{water} counterpart. As a result, the relaxivity of $[Mn(EDTA)]^{2-}$ at 20 MHz and 25 ºC (r_{1p} = 3.3 $mM^{-1}s^{-1}$) is somewhat lower than that of $[Gd(DTPA)]^{2-}$ (r_{1p} = 4.7 $mM^{-1}s^{-1}$).

Hydration number

The inner-sphere contribution to relaxivity is directly proportional to the number of coordinated water molecules *q* (Eq 8). Thus, a straightforward way to improve the relaxivities of Mn(II)-based contrast agents is to increase *q* through judicious ligand design. This strategy has been successfully applied to Gd(III) complexes, generally using potentially heptadentate ligands that leave two positions available to water molecules (i. e. AAZTA, see Figure 5).[23] Two main problems may arise upon decreasing the ligand denticity to allow the coordination of two water molecules: 1) This is generally accompanied by lower thermodynamic stability and kinetic inertness with respect to complex dissociation, and 2) The more open structure of the complex may result in the coordination of endogenous ligands (i. e. carbonate or phosphate), which replace the coordinated water molecules.[24]

The effect of an increased hydration number is clearly reflected in the relaxivities of the [Mn(DPAMeA)] and $[Mn(EDTA)]^{2-}$ complexes (Figure 5).[25,18] The ^{1}H NMRD profiles (Figure 4) evidence a higher relaxivity of [Mn(DPAMeA)] over the entire proton Larmor frequency range, which is mainly associated to the higher *q* value. The relaxivity gain at 20 MHz and 25 ºC amounts to 65%, resulting in a proton relaxivity (r_{1p} = 5.4 mM^{-1} s^{-1}) higher than those of commercially available Gd(III)-based contrast agents (i. e. r_{1p} = 4.7 mM^{-1} s^{-1} for $[Gd(DTPA)]^-$). This relaxivity increase is however accompanied by a significant drop of the thermodynamic stability of the complex (see below).

The determination of the hydration number of Mn(II) complexes is not straightforward. Caravan has proposed a method based on ^{17}O NMR measurements that can be applied to systems showing a maximum in the ^{17}O relaxivity as a function of temperature.[26] More recently Geraldes et al. proposed a more general method based

on ^{1}H NMRD measurements.[27] These authors derived an empirical formula that correlates the relaxivity measured at 0.01 MHz (and 25 ^{o}C) and the molecular weight (*FW*) of the complex:

$$q = \frac{r_{1p}}{9.16\left\{1-e^{\left(-2.97\times FW\times 10^{-3}\right)}\right\}} \quad (13)$$

For example, the relaxivities of [Mn(DPAMeA)] and [Mn(EDTA)]$^{2-}$ at 0.01 MHz and 25 ºC are 5.4 and 11.3 mM^{-1} s^{-1} (Figure 4). Application of Eq (13) provides hydration numbers of 1.9 and 0.9, respectively.

Electronic relaxation

Electronic relaxation is the main factor that controls the relaxivity at low magnetic fields (< 1 MHz). The relaxation of the electron spin is generally assumed to be the consequence of fluctuations of the zero field splitting (ZFS) energy caused by transient distortions of the metal coordination environment (transient ZFS), or by the so-called static ZFS contribution. The inspection of the low-field region of the ^{1}H NMR profiles of [Mn(EDTA)]$^{2-}$ and [Gd(DTPA)]$^{2-}$ suggests similar electronic relaxation. The analysis of the data provided values of the mean square zero-field-splitting energy of Δ^2 = 6.9×10^{19} s^{-2} and 4.4×10^{19} s^{-2}, which confirms the qualitative predictions obtained after inspection of the NMRD profiles. A slower electronic relaxation results in higher relaxivity values in the low-field region, as can be observed by comparing the ^{1}H NMRD profiles of the monohydrated complexes [Mn(DO1A)]$^+$ and [Mn(NOMPA)]$^+$ (Figure 6).[28, 18] While the relaxivity of [Mn(NOMPA)]$^+$ is also higher at fields > 10 MHz, the difference in the relaxivities of the two complexes is clearly larger at low fields (< 1 MHz). The fit of the data provided Δ^2 = 13×10^{19} s^{-2} and 3.7×10^{19} s^{-2} for [Mn(DO1A)]$^+$ and [Mn(NOMPA)]$^+$, respectively, which suggests that the lower relaxivity observed at low field for [Mn(DO1A)]$^+$ is related to a larger ZFS energy.

Rotational correlation time

The values of τ_m and τ_R determine the inner-sphere contribution to relaxivity at high fields (> 10 MHz). In most cases, the relaxivities of small Mn(II) and Gd(III) complexes are limited by the fast rotation of the complexes in solution. Thus, a straightforward manner to improve the relaxivities of both Mn(II) and Gd(III) complexes consists in slowing down the rotation of the complex, for instance by increasing the molecular weight of the complex or by covalent or non-covalent binding to macromolecules or nanoparticles. The effect that increasing τ_R has on the observed relaxivity can be easily visualized by comparing the relaxivities of the bis-aquated complex [Mn(DPAMeA)] and the binuclear and trinuclear derivatives *m*X(Mn(DPAMA))$_2$ and *m*X(Mn(DPAMA))$_3$, which present relaxivities at 20 MHz and 37 ºC of 4.2, 6.1 and 8.3 mM^{-1} s^{-1}, respectively, with τ_R values obtanined from the analysis of the corresponding NMRD profiles of 48, 96 and 136 ps.[29] A similar effect is observed by comparing the relaxivities of [Mn(HBzEDTA)]$^-$ and the hexameric analogue containing a cyclotriphosphazene core [N$_3$P$_3$(Mn(HBzEDTA))$_6$]$^{6-}$, which present relaxivities of 3.6 and 8.2 mM^{-1} s^{-1} at 20 MHz and 37 ºC, associated to τ_R^{310} of 80 and 450 ps, respectively.[30] The relaxivities of these medium-sized Mn(II) chelates are considerably higher than those of small complexes such as [Mn(EDTA)]$^-$ or commercially available contrast agents such as [Gd(DOTA)]$^-$ (Figures 5 and 7).

Another strategy relies in the formation of micelles in solution, promoted by the amphiphilic nature of the complexes. This strategy has been exploited to improve the relaxivities of Gd(III) complexes, and more recently those of Mn(II)

analogues.[31-33] This is illustrated by the NMRD profiles of [Mn(DPAC12A)] recorded above and below the critical micellar concentration, which was determined to be 96 μM (Figure 8). The formation of micelles slows down the rotation of the complex in solution, which is evidenced by the presence of a bump in the NMRD profile with a maximum at about 40 MHz. A further increase in relaxivity is observed upon binding of [Mn(DPAC12A)] to Human Serum Albumin (HSA), which has been characterized by an affinity constant 1.3×10^5 M^{-1}.[33]

According to the Debye-Stokes equation, a linear relationship is expected between the molecular weight of the complex and τ_R. However, this linear dependence does not hold for slowly tumbling systems due to the contribution of both local and global motions. The model-free Lipari-Szabo approach[34, 35] accounts for this effect by rewriting Eq (9) as:

$$\left(\frac{1}{T_{1m}^H}\right)^{DD} = \frac{2}{15}\left(\frac{\mu_0}{4\pi}\right)^2 \frac{\gamma_I^2 g^2 \mu_B^2}{r_{MnH}^6} S(S+1)\left[\frac{3S^2\tau_{d1g}}{1+\omega_I^2\tau_{d1g}^2} + \frac{3(1-S^2)\tau_{d1}}{1+\omega_I^2\tau_{d1}^2} + \frac{7S^2\tau_{d2g}}{1+\omega_I^2\tau_{d2g}^2} + \frac{7(1-S^2)\tau_{d2}}{1+\omega_I^2\tau_{d2}^2}\right] \quad (14)$$

$$\frac{1}{\tau_{dig}} = \frac{1}{\tau_m} + \frac{1}{\tau_{RG}} + \frac{1}{T_{ie}} \qquad i = 1, 2 \quad (15)$$

$$\frac{1}{\tau_{di}} = \frac{1}{\tau_m} + \frac{1}{\tau} + \frac{1}{T_{ie}} \qquad i = 1, 2 \quad (16)$$

$$\frac{1}{\tau} = \frac{1}{\tau_{RG}} + \frac{1}{\tau_{RL}} \quad (17)$$

Where τ_{RG} represents the correlation time describing the rotational motion of the entire molecule, while τ_{RL} is the correlation time associated with the local rotational motion. S^2 is the generalized order parameter and accounts for the degree of coupling between the two types of motion. The S^2 parameter assumes the value 0 for completely independent motions and the value of 1 when local and global motions are fully correlated. A typical example of an analysis using the Lipari-Szabo model is given by the [Mn(DPAC12A)] complex. Below the cmc the ^{1}H NMRD data can be perfectly fitted without separating the local and glogal motions, using a τ_R value of 123 ps (Table 2). Above the cmc the Lipari-Szabo model provides a long τ_{RG} value of 5.5 ns and a short τ_{RL} value characterising the fast local motion, which is limiting the observed relaxivity due to the rather low S^2 value of 0.26. Binding to HSA results in a higher relaxivity, which is related mainly to a loger τ_{RL} value associated to an increased local rigidity.

Water exchange lifetime τ_m

The exchange rate of the coordinated water molecules determined for the aquated Gd(III) ion $[Gd(H_2O)_8]^{3+}$ is very fast, with a mean residence time of τ_m^{298} = 2.5 ns. In complexes other than the aqua ion, water exchange is generally slower, expanding a range of about four orders of magnitude (τ_m^{298} from 20 μs to 2.5 ns). The mean residence time of a water molecule in $[Mn(H_2O)_6]^{2+}$ is considerably longer (τ_m^{298} = 35.5 ns), but water exchange is generally accelerated by coordination of polydentate ligands. As a result, the ranges of τ_m values reported for Gd(III) and Mn(II) complexes largely overlap (τ_m values in the range 0.8 μs to 0.2 ns have been reported for Mn(II) complexes).[36] In the case of Gd(III), water exchange can be modulated in a rational way thanks to very exhaustive studies correlating τ_m with factors such as ligand architecture, complex charge and steric compression around the water binding site. Most Gd(III) complexes studied in the context of potential MRI contrast agents are nine-coordinated species for which water exchange follows a dissociative (or dissociative interchange) mechanism. However, the situation is more intricate for Mn(II) complexes,

which typically present six- or seven-coordinated ions in solution. As a result, both dissociatively and associatively activated exchange mechanisms are likely playing a role. Nevertheless, some general trends can be established. Water exchange in seven-coordinated Mn(II) complexes is generally slowed down by increasing the positive charge of the complex, as it is evident by comparing the τ_m values determined for [Mn(1,4-DO2A)] and [Mn(1,4-DO2AM)]$^{2+}$, which were found to be τ_m^{298} = 0.9 and 8.7 ns, respectively (Figure 9).[37, 18] This can be attributed to a stronger bond between the metal ion and the coordinated water molecule as the positive charge of the complex increases, which increases the activation barrier to reach the six-coordinate transition state following a dissociative mechanism. A similar effect is likely responsible for the slower water exchange rate measured for [Mn(PyC3A)]$^-$ (τ_m^{298} = 18.5 ns)[38] compared to [Mn(EDTA)]$^{2-}$ (τ_m^{298} = 2 ns). The effect of complex charge is however reversed in the case of six-coordinate species, which are expected to present an associatively activated water exchange mechanism. For instance, the τ_m^{298} value reported for [Mn(12-pyN4A)(H_2O)]$^+$ (τ_m^{298} = 0.3 ns) evidences a faster water exchange reaction than that measured for the charge-neutral analogue [Mn(12-pyN4P)(H_2O)] (τ_m^{298} = 0.6 ns).[39] In this case the positive charge of the complex probably facilitates the coordination of the entering water molecule following an associative water exchange reaction. Nevertheless, water exchange rates in Mn(II) complexes are generally in the same order of magnitude of the aqua ion or above. As a result, water exchange is not expected to limit ^{1}H relaxivity even for slowly tumbling systems.

Stability and Safety of Mn(II)-based contrast agents

Mn(II) is an endogenous metal ion present in serum at a concentration of 0.5–1.2 µg/L. It is an essential ion for normal development and body function; it functions as an enzyme activator and as a constituent of metalloenzymes, *i.e.* manganese superoxide dismutase (SOD) or glutamine synthetase.[40] However, it must be highlighted that large doses of Mn(II) are neurotoxic (LD_{50} = 0.22 mmol/kg for rat) and its accumulation in brain may cause manganism, a neurological disorder similar to Parkinsonism, likely caused by the damage of basal ganglia and, in particular, of the globus pallidus.[41, 42]

Mn(II)-based MRI contrast agents consist of a chelate between Mn(II) ions and a polydentate polyaminocarboxylate ligand. A detailed study of the thermodynamic stability and kinetic inertness of these chelates is critical to ensure a safe *in vivo* application of such CAs.[43] In general, the thermodynamic stability of Mn(II) complexes is lower compared with that of other transition-metal or Gd(III) complexes, mainly due to the smaller charge of the Mn(II) ion and to the lack of ligand-field stabilization energy associated with its high-spin d^5 electron configuration. In terms of kinetic inertness, the rates of both transmetallation reactions with endogenous ions like Ca(II), Zn(II), and Cu(II) and proton-assisted dissociation are crucial because these reactions may result in the formation of free metal ion and/or free ligand, both toxic for the organism. The stability and kinetic data for Mn(II) complexes are not as complete as in case of Gd(III) systems, but many data are now available for both acyclic and macrocyclic Mn(II) complexes. Typically, acyclic chelates are more labile than macrocyclic ones, being one striking example [Mn(DTPA)]$^{3-}$, which was found to dissociate almost instantaneously (ca. 8 ms) in the presence of Cu(II) ions.[44] Conversely, macrocyclic systems are more inert, although

the compromise between high ligand denticity, necessary to form stable complexes, and the need to have a water molecule coordinated to the paramagnetic centre, may lead to Mn(II) complexes not sufficiently stable. Herein, we will discuss separately the Mn(II) complexes formed with acyclic and macrocyclic ligands.

Mn(II) complexes with acyclic ligands

The most investigated among the linear ligands for Mn(II) complexation is EDTA which forms the relatively stable 7 coordinate $[Mn(EDTA)]^{2-}$ complex ($\log K_{ML}$ = 13.88, pMn = 7.95 at pH 7.4) in which a water molecule occupies the seventh coordination site. The relaxivity of $[Mn(EDTA)]^{2-}$ is 3.3 $mM^{-1}s^{-1}$ (298 K, 20 MHz), typical of q = 1 small molecular weight Mn(II) complexes.[18] The coordinated water molecule is in fast exchange with bulk water (k_{ex} = 4.7 ×10^8 s^{-1}) making it possible to achieve high relaxivities when the rotational dynamics of the complex is markedly slowed down (long τ_R) following a conjugation or interaction with slowly tumbling substrates, *i.e.* in aggregated form (micelles) or bound to human serum albumin (HSA). In particular, EDTA-like ligands embodying one or two aliphatic chains on the ethylene backbone have been recently used to prepare amphiphilic Mn-complexes able to aggregate in micellar structures in water or by mixing them with pegylated phospholipids.[31] The relaxivity values obtained by these nanosized systems were interesting, especially for the system containing two aliphatic chains that partially block the local rotation of the chelate once the system is embedded in the lipidic nanoparticle (r_{1p} = 18.4 $mM^{-1}s^{-1}$ at 298 K, 20 MHz). The same Mn(II) complexes formed strong adducts with HSA (K_A ~ 10^5) and r_1^b values up to 61.5 mM^{-1} s^{-1} were obtained, with a twenty-fold increase with respect to the r_1 of Mn(EDTA), as in the case, for example, of $Mn(EDTAC_{16})$.[31]

Other MnEDTA-like chelates containing chemical groups known to promote a noncovalent binding interaction to HSA were reported in the literature: MnEDTA-BOM and $MnEDTA\text{-}BOM_2$, bearing one or two benzyloxy groups, whose HSA adducts gave r_1^b values of 55.3 and 48.0 mM^{-1} s^{-1} (20 MHz and 298 K).[45] Moreover, an EDTA derivative linked through a phosphodiester spacer to a diphenylcyclohexyl group, the identical moiety used in the Gd-based CA MS-325, was reported to achieve r_1^b values of 46–51 mM^{-1} s^{-1} (at 310 K), depending of the type of serum used.[46] The r_1^b values of the adducts HSA-MnEDTA-like complexes are higher than the majority of the monoaquo Gd-based blood pool CAs, most probably as a result of the fast exchange condition of the inner sphere water molecule. Finally, lower values were reported for the MnEDTA-like complex bearing a deoxycholic moiety interacting with HSA (r_1^b = 32.7 mM^{-1} s^{-1} at 20 MHz and 298 K).[47] However, although several promising MnEDTA-based CAs have been proposed, the kinetic inertness of $[Mn(EDTA)]^{2-}$ is quite low due to the flexibility of the open-chain ligand. In fact, the half-life ($t_{1/2}$) of the dissociation reactions of $[Mn(EDTA)]^{2-}$, calculated at physiological conditions (pH = 7.4 and at 1 × 10^{-5} M concentration of the exchanging Cu(II) ion), has been determined as only 4.56 min.[44]

For this reason, the more rigid EDTA analogue *trans*-1,2-CDTA was proposed for Mn(II) complexation as it exhibits a constrained structure and a pre-organized cavity which is particularly suitable for the coordination of the metal-ion (Figure 5). The presence of the cyclohexyl ring in place of the ethylene backbone has been found to improve by four orders of magnitude the kinetic inertness of Mn(II) in the presence of competing metal ions ($t_{1/2}$ of $[Mn(CDTA)]^{2-}$ = 12 h in the same conditions reported above.[44] Moreover, the thermodynamic stability constants increased of one order of

magnitude with respect to $[Mn(EDTA)]^{2-}$. An improved CDTA derivative bearing a picolyl pendant arm in place of an acetic arm has been recently proposed (PyC3A).[38] The pyridyl-*N*-donor was incorporated in order to impart further rigidity and increase the lipophilic character of the Mn(II) complex. In terms of thermodynamic stability, $[Mn(PyC3A)]^{-}$ showed $\log K_{ML}$ = 14.14 and pMn = 8.2, slightly lower than those of $[Mn(CDTA)]^{2-}$, and improved kinetic inertness with respect to $[Mn(CDTA)]^{2-}$. In terms of relaxometric behaviour, $[Mn(CDTA)]^{2-}$ maintains the coordinated water molecule in the inner sphere and thus a r_{1p} value of 3.62 mM^{-1} s^{-1} (20 MHz, 298 K) with a ca. 10% increase with respect to $[Mn(EDTA)]^{2-}$ due to the increased molecular weight.[48] Contrarily, the r_{1p} reported for $[Mn(PyC3A)]^{-}$ is 2.1 mM^{-1} s^{-1} (60 MHz, 310 K) quite low for a q = 1 Mn(II) complex. However, the temperature dependence of bulk water ^{17}O T_2 demonstrated that an inner-sphere water co-ligand is present. $[Mn(PyC3A)]^{-}$ was also tested *in vivo* providing excellent MR contrast and showing an elimination from the body via renal and hepatic pathways.[49] Thus, a bifunctional derivative was synthesized and two dimeric units of $[Mn(PyC3A)]^{-}$ were conjugated to a fibrin binding peptide to form a tetrameric probe able to show strong enhancement of carotid artery thrombosis. The four-fold increase in relaxivity and the *in vivo* stability and whole body Mn clearance of this tetrameric probe makes $[Mn(PyC3A)]^{-}$ a promising system for MRI applications.[38] A series of ligands having a hydroxybenzyl pendant arm in place of an acetic arm of EDTA (HBET) and CDTA (CyHBET) were also reported to form stable complexes with Mn(II) and Mn(III) ions.[50, 51] $[Mn(HBET)]^{2-}$ and $[Mn(CyHBET)]^{2-}$ complexes were proposed as redox activated MRI CAs since the phenolate donor favours the oxidation of Mn(II) to Mn(III) and thus the passage from coordination number (CN) 7 and q =1 with Mn(II) to CN 6 and q = 0 with Mn(III). The relaxivities of the Mn(II)-HBET and Mn(III)-HBET complexes at 1.4 T and 310 K are 2.76 and 1.05 mM^{-1} s^{-1}, confirming the q = 1 and q = 0 states, respectively. In case of $[Mn(CyHBET)]^{2-}$, the $\log K_{ML}$ is almost the same as that reported for $[Mn(PyC3A)]^{-}$, although pMn is much lower (6.7 vs 8.2, respectively) due to the increased basicity of the ligand. The relaxometric results show r_1 values of 3.3 and 0.4 mM^{-1} s^{-1} for $[Mn(CyHBET)]^{2-}$ and $[Mn(CyHBET)]^{-}$, respectively. Interestingly, when the phenol group is deprotonated (*i.e.* above pH 8, the pK_a are *ca.* 7.3-7.4) the rate of water exchange for these type of Mn(II) complexes is very fast, between 4 and 7 × 10^9 s^{-1}, whereas in the protonated form the k_{ex} is smaller than that measured for $[Mn(EDTA)]^{2-}$ (in the order of 0.5 - 1 × 10^8 s^{-1}). With the aim to find an optimized reversibly activated Mn(II/III) MR imaging probe, electron withdrawing (NO_2) or donating (OCH_3) groups in para-position to the phenolic OH were introduced allowing a modulation of both thermodynamic and relaxometric properties of the Mn^{II} complexes and also of the redox potential of the Mn(II/III) couple.[51]

Moving to structurally different ligands, the hexadentate derivatives of AAZTA (6-methyl-1,4-perhydrodiazepine tetraacetic acid) having an acetate pendant arm removed, AAZ3A, MeAAZ3A, and AAZ3MA, were reported to form Mn(II) complexes with conditional stability pMn in the order of 9. The analysis of the relaxometric and ^{17}O NMR spectroscopic data revealed an equilibrium between the mono- and non-hydrated Mn(II) complexes depending on the substitution of acetic pendant arms and/or of the exocyclic amino group. These q = 1/q = 0 equilibria are also reflected in the r_{1p} values measured at 20 MHz and 298 K that ranges between 2.5 and 1.9 mM^{-1} s^{-1}, as well as in the $^{298}k_{ex}$ values that lie between 4.7 and 13.3 × 10^7 s^{-1}.[52]

Chelating ligands containing picolinate pendant arms are another type of systems that demonstrated excellent coordinating ability towards Mn(II). In particular, a family of pentadentate 6,6'-((alkylazanediyl)bis(methylene)) dipicolinic acid (DPAA) ligands were developed where different substituents are attached at the amine nitrogen atom: acetate, methyl, phenyl, dodecyl and 4-hexylphenyl.[25, 33] The q=1 $[Mn(DPAAA)]^-$ complex exhibited a good thermodynamic stability ($\log K_{MnL}$ = 13.19), sensibly higher than that of the q=2 [Mn(DPAMeA)] and [Mn(DPAPhA)] analogues ($\log K_{MnL}$ = 10.13 and 9.55, respectively). Also the r_{1p} values (20 MHz, 298 K) varies as a function of the number of coordinated water molecules, being 3.5 mM^{-1} s^{-1} for $[Mn(DPAAA)(H_2O)]^-$ and 5.3 and 6.6 mM^{-1} s^{-1} for the two bis-hydrated complexes. In terms of k_{ex}, the values found for these complexes are in the range 5.6 - 30.6 × 10^7 s^{-1}, lower than the exchange rates measured for $[Mn(EDTA)]^{2-}$. The dodecyl lipophilic chain present on [Mn(DPAC12A)] favoured the formation of micelles in solution with relaxivity of 8.5 mM^{-1} s^{-1}. Both lipophilic $[Mn(DPAC_6PhA)]$ and $[Mn(DPAC_{12}A)]$ derivatives were found to have a good affinity for HSA with association constants of 7.1 × 10^3 and 1.3 × 10^5 M^{-1} and r_1^b of 45.5 and 15.5 mM^{-1} s^{-1}, respectively.

Mn^{II} complexes with macrocyclic ligands

A picolinate pendant arm was also attached to macrocyclic polyamines, such as tacn, cyclen and cyclam, to obtain penta- and hexadentate ligands able to form efficient Mn(II) complexes.[26] In aqueous solution, these ligands form thermodynamically stable complexes with $\log K_{MnL}$ = 10.28 (nompa), 14.48 (dompa), and 12.53 (tempa). Unfortunately, a fast spontaneous dissociation of the complexes at pH 7.4 was found to occur for all complexes, probably due to the presence of two or three secondary amines of the macrocycles that can be easily protonated accelerating the decomplexation reaction. The relaxivity of Mn(dompa) and Mn(tempa) showed the absence of inner-sphere water molecules (r_{1p} = 1.3 and 1.2 mM^{-1} s^{-1}), whereas in Mn(nompa) the Mn(II) ion is reported to be six-coordinate with one coordinated water molecule. From the analysis of the NMRD and ^{17}O NMR data a fast water exchange rate ($^{298}k_{ex}$ = 2.8 × 10^9 s^{-1}) was determined.

A macrocyclic core that was variably functionalized in order to form chelating ligands very efficient for Mn(II) complexation is pyclen ([12]pyN4). Mono-functionalization with acetic or methylphosphonic pendant arm gave pentadentate ligands that formed mono-aqua Mn(II)-complexes (CN 6) with good stability (pMn slightly above 8) and kinetic inertness lower than $[Mn(CDTA)]^{2-}$ ($t_{1/2}$ = 144 min, pH 7.4, $[Zn^{2+}] = 10^{-5}$ M).[39] In terms of relaxometric behaviour, the two complexes showed an r_1 value of 2.39 and 2.84 mM^{-1} s^{-1} (20 MHz, 298 K) and $^{298}k_{ex}$ of 3 × 10^9 and 1.8 × 10^9 s^{-1} for the mono-acetic and mono-phosphonic derivatives, respectively. A series of tris-amide pyclen derivatives and their Mn(II) complexes have also recently been reported and compared to the triacetate analogue (PCTA) with the aim to gain several different information, especially on how the nature of the pendant donor groups influence the thermodynamic stability and kinetic inertness of the complexes.[53] From a relaxometric point of view, all ligands are heptadentate, therefore they form low relaxivity q = 0 Mn(II) complexes (in the range 1.2-1.5 mM^{-1} s^{-1}). The presence of seven donor atoms and the macrocyclic structure allowed to form very stable and very inert complexes with an increase in half-life $t_{1/2}$ passing from negatively charged carboxylate to neutral amide donors.

Moving to cyclen-based ligands (cyclen = 1,4,7,10-tetraazacyclododecane) our group investigated in detail a series of Mn(II) complexes with ligands bearing one, two, and three acetate pendant arms (DO1A, 1,4- and 1,7-DO2A, and DO3A, respectively) by ^{1}H and ^{17}O NMR relaxometry and computational studies.[18] In particular, the Mn(II) complex with the pentadentate DO1A ligand contains one bound water molecule (q = 1), whereas Mn(DO3A) is a q = 0 and their r_{1p} values are 2.4 and 1.3 mM^{-1} s^{-1}, respectively. The Mn(II) complexes of the isomeric 1,7- or 1,4-DO2A di-substituted ligands presented two different coordination numbers and therefore a different q: CN6 and q = 0 for Mn(1,7-DO2A) and predominantly CN7 and q =1 for Mn(1,4-DO2A). Specifically, Mn(1,4-DO2A) is present in solution as a mixture of seven- (ca. 87 %) and six-coordinate species (ca. 13 %) differing in the number of coordinated water molecules, one and zero respectively. The higher relaxivity of Mn(1,4-DO2A) as compared to Mn(1,7-DO2A), 2.1 vs 1.5 mM^{-1} s^{-1} at 20 MHz and 298 K, is a consequence of the different population of the mono-hydrated species. In terms of thermodynamic and kinetic properties of these cyclen-based Mn(II) complexes, the measured stability constants of [Mn(1,4-DO2A)] and [Mn(1,7-DO2A)] have very similar values (log K_{MnL} = 15.68 and 15.22, respectively).[54] Conversely, the dissociation half-lives ($t_{1/2}$) of the Mn(II) complexes determined at physiologically pH (at pH= 7.4) are slightly higher for [Mn(1,7-DO2A)] (57 h vs 48 h for [Mn(1,4-DO2A)]). When the two acetic pendant arms in 1,4 position were replaced by two *N*,*N*-dimethylacetamide pendants, the water exchange rate of the Mn(II) complex is one order of magnitude slower than that of [Mn(1,4-DO2A)] ($^{298}k_{ex}$ = 1.15 × 10^{8} s^{-1}) and the relaxivity slightly higher (+20 %, r_{1p} = 2.5 mM^{-1} s^{-1}, 20 MHz, 298 K). Interestingly, Mn(1,4-DO2AM) showed an improved kinetic inertness, reaching a half-life of 556 h at pH 7.4.[37] This property has been attributed both to the formation of a positively charged Mn(II) complex, which hinders the protonation and then the acid-catalysed dissociation, and to the low basicity of the amide oxygen atom that does not promote the proton transfer to the ring nitrogen atom. Similarly to EDTA, also 1,4-DO2A and 1,4-DO2AM were modified by inserting lipophilic groups with the aim to allow the formation of aggregated lipidic nanoparticles and or supramolecular adducts with HSA.[31, 32] Thus, the Mn(II) complexes of two 1,4-DO2A derivatives with dodecyl and hexadecyl chains attached on the free secondary amines of DO2A were prepared and the aggregated micellar forms in the presence of pegylated phospholipids were investigated.[31] The relaxivities at 20 MHz and 298 K were 12.6 and 15.3 mM^{-1} s^{-1} for the bis-C_{12} and bis-C_{16} DO2A derivatives, respectively, lower than that found for the mixed micelles of MnEDTA-bis-C_{16} (18.4 mM^{-1} s^{-1} in the same experimental conditions). The interaction of these amphiphilic Mn(II) complexes with HSA was also investigated by ^{1}H NMR relaxometry giving rise to association constants K_A in the order of 10^{4} M^{-1}. The r_1^b of these adducts were 29.5 and 27.2 mM^{-1} s^{-1} for the bis-C_{12} and bis-C_{16} DO2A derivatives, respectively (20 MHz, 298 K). These values are substantially lower than the correspondent MnEDTA-bisC_{12}-HSA system, most likely because of a lower hydration state of Mn(1,4-DO2A)-like complexes that maintain the q = 1 / q = 0 equilibrium that reduces the possible r_{1p} enhancement. Nevertheless, these amphiphilic MnDO2A-like complexes present slightly higher r_1^b values of the HSA adducts than those reported in the literature for similar systems. In particular, the adducts between HSA and the bis-amide di-benzyl derivatives Mn-1,4-DO2AMBz and Mn-1,4-BzDO2AM, showed r_1^b of 27.4 and 18.3 mM^{-1} s^{-1}, respectively.[32] The reason lies in the stronger interaction with HSA of the long and adjacent carbon chains

with respect to the benzyl moieties and thus to a more efficient restriction of the local rotation of the complex, thus favouring higher relaxivities.

Mn(II)-based nanoprobes

More recently, specific attention was also devoted to the design of novel efficient Mn(II)-based nanoparticles, aiming to increase the relaxivity performance and to reduce the concentration of Mn(II) to administrate to a patient. Some specific aspects of relaxation enhancement in Gd- and Mn-based nanosized systems have been discussed in detail recently.[55-56] Different synthetic strategies have been proposed in the literature and they can be summarised in the following points: *i*) Anchoring and intercalation of discrete Mn(II) chelates in silica and layered materials; *ii*) inclusion of Mn(II) ions in the inorganic framework of mesoporous silica nanoparticles; *iii*) preparation of MnO and manganese phosphate nanoparticles.

i) *Anchoring and intercalation of discrete Mn(II) chelates in silica and layered materials*

A very recent example of microporous silica functionalized with Mn(II) chelates was proposed by Z. Varga et al.[57] The authors prepared an organo-modified silica, functionalized on the surface with amino groups and characterized by a porosity suitable to confine large amount of Mn(II) complexes. The amino groups were exploited to promote the chemical attachment of MnDTPA complexes (Figure 10). The nanospheres showed good colloidal stability in aqueous solution and after administration in mouse they exhibited marked liver-specific T_1-weighted MRI contrast with a longitudinal relaxivity value at 1 T of ca. 7.2 mM^{-1} s^{-1}, significantly higher than typical low molecular weight Mn(II) chelates (Fig. 10).

In 2016, negative charged Mn(II) aminophosphonates, prepared by reaction of the polyaminophosphonate ligand and MnO, were intercalated in the interlayer space of layered double hydroxides solids (LDHs). These layered materials are composed by positively charged metal hydroxide layers and a interlayer populated by different anions, which can be opportunely replaced by anionic complexes. In the work of Geraldes et al, a biodegradable $[Zn_5(OH)_8]Cl_2{\cdot}yH_2O$ (Zn_5-Cl) LDH was used as host material.[58] The complexes selected in the work present a number of inner sphere water molecules from 0 and 1 and a strong contribution of second sphere. The relaxivities of the intercalated solids showed lower relaxivity values in comparison to the discrete chelates. This result was mainly ascribed to both a steric effect of the complexes located into the interlayer space and to a replacement of the inner sphere water molecules form carbonates groups. Nevertheless, both longitudinal and transversal relaxivity values at 20 MHz and 37°C are sufficiently enough to justify a possible use of these materials as MRI contrast agents.

ii) *Inclusion of Mn(II) ions in the inorganic framework of mesoporous silica nanoparticles*

The first mesoporous silica functionalized with Mn(II) ions was obtained through an in-situ chemical oxidation–reduction process.[59] Nevertheless, in this case the $1/T_1$ relaxivity measured at 3T for an aqueous solution of the calcined and reduced sample was lower when compared to parent samples containing Gd(III) in the framework. Later, in 2013, M.-A. Fortin et al., developed, through incipient wetness synthesis, a porous 3D silica functionalized with Mn(II) ions with

better relaxometric performances (Fig. 11).[60] Following this approach, Mn(II) ions are homogeneously distributed in the silica framework and they are more accessible to the water molecules. For these reasons, the final material showed higher longitudinal relaxivity value, respect to parent samples (8.4 mM^{-1} s^{-1} at 1.5 T), good chemical stability and appreciable MRI contrast ability. Another example of mesoporous silica nanoparticles containing Mn(II) was proposed by J. Shi et al. This material was suggested as promising dual-mode contrast agent for simultaneous T_1- and T_2-weighted MR imaging because of the large values of the longitudinal (r_1 = 10.1 mM^{-1} s^{-1}) and transverse (r_2 = 169.7 mM^{-1} s^{-1}) relaxivity at 3T, comparable or higher than the typical values of the clinically used Gd(III) chelates and iron oxide nanoparticles, respectively.[61]

iii) *Preparation of MnO and manganese phosphate nanoparticles*

MnO nanoparticles were proposed as alternative to typical Mn(II) chelates, because of their ability to contain a large amount of accessible Mn(II) ions able to reduce the relaxation time of the protons of water molecules. Staring from these results, different examples of functionalized MnO nanoparticles were studied in the literature aiming to further improve the relaxivity performance of these systems.[62] Data in the literature demonstrated that a proper modification of the particles size and morphology is useful to influence the longitudinal relaxivity values. For instance, ultra-small nanoparticles, characterized by high surface-to-volume ratio are very efficient as MRI contrast agents. A critical role is also played by the coating used to stabilize MnO nanoparticles. Unfortunately, the functionalization of the surface with polyethylene glycol or PLGA polymers is detrimental by the relaxometric point of view, because these kind of coatings limit the water access to the Mn(II) ions exposed on the particles surface. In opposite, the decoration of these nanoparticles with proteins or polyaspartic acid is the best strategy to increase the relaxivity to values in the range 1.2 - 2 mM^{-1} s^{-1} at 7 T (Fig. 12).[63] A recent study demonstrated that manganese oxides Mn_xO_y have interesting relaxation properties, with MnO_2 nano-urchins providing up to 140% signal enhancement.[64]

More recently, the inclusion of pre-formed MnO nanoparticles in mesoporous silica was also carried out. Li, Wang and co-workers developed a novel nanohybrid-encapsulated MnO NPs with a relatively high longitudinal relaxivity of ca. 1.2 $mM^{-1}s^{-1}$ at 7 T, as a consequence of the improved accessibility of the water molecules to the MnO nanoparticles. Moreover, good biocompatibility and chemical stability without metal leaching were also observe.[65]

Amorphous porous manganese phosphate nanoparticles have been also proposed in the literature as potential MRI and theranostic probes for biomedical applications. In 2017, Y. Hao et al. designed a multifunctional porous manganese phosphate containing a photosensitizer molecule (drug) for photodynamic therapy and functionalized on the surface with a pH-responsive linker, able to control the drug release. The r_{1p} relativity value measured at neutral pH was 1.9 $mM^{-1}s^{-1}$ at 0.5 T, in agreement with data observed for MnO nanoparticles. However, at acid pH, an improvement of the relaxivity associated to the Mn(II) release in aqueous solution was observed.[66]

Preclinical application of Mn(II)-based probes

Despite the thirty year clinical use of Gd(III)-based CAs, Mn(II) agents have only scarcely been used in clinics. Only one Mn(II) complex was clinically approved for intravenous use (TESLASCAN®, MnDPDP) as liver imaging agent;[67] however, this Mn-agent was withdrawn from the US market in 2003 and the European market in 2012. This *q* = 0 complex slowly releases the metal ion *in vivo* and, thus, most of the relaxation enhancement is provided by the free metal ion or the metal ion interacting with endogenous proteins.[68] The search for more kinetically inert Mn(II) complexes has provided much safer alternatives for targeted probe development and some preclinical studies have been recently reported. As anticipated in the previous sections, the group of Caravan has recently tested *in vivo* the small chelate $[Mn(PyC3A)]^-$ and suggested its use for contrast-enhanced MR angiography.[38, 49] After i.v. injection, they highlighted an initial blood pool enhancement and a rapid clearance of the compound from the blood via a mixed renal/hepatic pathway. The intravascular contrast enhancement and the pharmacokinetics of $[Mn(PyC3A)]^-$ are comparable to those of the commercially available $[Gd(DTPA)]^{2-}$ CA. Moreover, a HPLC-MS study showed that Mn-PyC3A is excreted intact without undergoing metabolism or degradation. $[Mn(PyC3A)]^-$ was also used for MR-imaging of the Central Nervous System (CNS) on baboons on a clinical 3T a scanner and compared directly to GdDTPA using the same dose, formulation, injection rate, and scanning protocol.[69] The observed values of the artery-to-muscle contrast-to-noise ratio (CNR) between images obtained using Mn(PyC3A) or GdDTPA did not show a statistical difference (Figure 13). Thus, based on the similar contrast and pharmacokinetic properties of Mn(PyC3A) and GdDTPA, the authors concluded that the Mn(PyC3A) complex represents a suitable CA for visualization of CNS lesions. The same agent, in a dimeric form, was also conjugated to both end of a fibrin-targeted peptide to detect carotid artery thrombosis in a rat model. An 80% increase in signal to noise ratio in the thrombus is clearly an indication of probe accumulation in the site of interest. In addition, there was an increase of more than five times after injection of the thrombus-to-muscle CNR that was maintained throughout the duration of the study. *In vivo* stability and total body Mn clearance of this tetranuclear complex added additional positive data suggesting that $[Mn(PyC3A)]^-$ may be a promising candidate for non-Gd MR applications. Finally, a library of lipophilic derivatives of PyC3A was synthesized and the liver uptake and rate of blood clearance for their Mn(II) complexes was tested.[70] In particular, the benzyloxy derivative was indicated as the most efficient due to a combination of high relaxivity, rapid blood clearance, and strong hepatocellular uptake. Evaluation of this liver specific Mn-agent in a murine liver tumour model showed evident hypo-intense signals corresponding to the tumor with an 83% liver parenchyma vs tumour CNR. Most importantly, ex-vivo quantitation of Mn content showed complete elimination of Mn within 24 h after injection. This latter property was claimed to ameliorate the behaviour of another agent based on a Mn(II) complex of an EDTA chelate conjugated to a benzothiazole aniline moiety that was also recently reported as liver-specific agent. In fact, this agent was shown to provide strong delayed phase liver enhancement but more than 50% of the injected Mn is retained in mice 24 h after injection.[71]

With regard to Mn-based nanoparticles and macromolecular agents, the review from Lanza et al. [72] have reported a comprehensive account of the preclinical studies carried out on Mn-Doped FeO nanoparticles, Mn-oxide, Mn-based organic or polymeric NPs or clusters. However, it has been highlighted that nanotoxicity,[73] and especially

immunotoxicity,[74] has emerged as one of the critical issues to make NPs into practical clinical applications. Thus, although studies on more efficient MnO NPs both in terms of relaxivity and in vivo biocompatibility have been recently reported,[75, 76] the in-vivo biocompatibility, biodistribution, targeting efficiency, toxicity and clearance of MnO NPs is still under investigation before their safe use into clinical trials. Such properties are, in fact, strongly correlated to morphology, particles size and surface reactivity of these materials.[63]

Future Perspective

In this review, we have summarized the strategies for the design and optimization of Mn(II) probes for MRI imaging applications. Manganese(II) complexes have excellent potential as alternative MRI contrast agents to Gd-based probes due to their favourable relaxometric properties and good biochemical characteristics. Despite the lower magnetic moment, the shorter Mn-O distance of bound water and its generally high exchange rate favour fully comparable relaxivity values. However, although studies on Mn (II) complexes have grown considerably over the last few years, the number and type of chemical structures examined is still quite limited when compared to the Gd(III) compounds. The coordination chemistry of Gd(III) complexes and its relationship with their physico-chemical properties were examined in great detail in the past about three decades. Precise information was acquired on the solution structure of the complexes, their dynamic behaviour, the number of interconverting isomers, the processes of coordinated water exchange, the different ways to control the molecular tumbling and the state of hydration. In addition, the relevant aspects that define the thermodynamic stability and kinetic inertness of the complexes have been clarified, as well as transmetallation mechanisms and the formation of ternary compounds with biologically relevant oxyanions. All these results are the result of a systematic and very extensive investigation that involved the synthesis of a large library of chelators different in structure, number and type of donor groups.[77, 78]

A study of similar breadth and depth would be extremely useful also for the Mn(II) complexes. We could greatly benefit from a research that embraces structurally extremely different ligands, as it would help us to understand with greater breadth and depth the relationship between the chemical and structural features of the ligands and the thermodynamic, kinetic and relaxometric properties of the related Mn(II) complexes, in a manner similar to the case of Gd(III) systems. Clear improvements will be achieved by a wider selection of the donor groups and of the pendant arms of the ligand backbone. The type of donor atoms that bind to manganese ion influence inner-sphere water exchange and electronic relaxation, two key parameters that determine the relaxivity of the complexes. In addition to these molecular parameters also thermodynamic stability and kinetic inertia can be tuned by proper choice of donor atoms. This goal is certainly more difficult to realize than in the Gd (III) complexes, as an obvious consequence of the lower coordination number of Mn (II). However, some examples of stable complexes potentially suitable for in vivo studies have been reported recently. These results are very promising and clearly indicate the great potential of Mn(II)-based systems as MRI diagnostic probes.

Along with the significant progress in the development of low molecular weight complexes, the absorption, biodistribution, metabolism and clearance study of the probes, however, is still missing in the vast majority of studies. The lack of these data represents an obstacle on the way toward clinical translation of the newly developed systems. In the near future, a systematic study of the excretion, pharmacokinetics, and metabolism of the complexes will yield significant and important information.

As well established in the case of Gd(III) complexes, the conjugation of small metal chelates to macromolecular platforms induces considerable increases in relaxivity. The nanosystems are characterized by a high payload of paramagnetic centers, ideally each of them with an optimized r_1 value, which makes the value of relaxivity per particle extremely high, thus significantly reducing the detection limit. Even in the case of Mn(II), this strategy is effective and provides excellent results. Lipophilic complexes of Mn(II) have been incorporated into micellar systems and liposomes or non-covalently conjugated to serum albumin. Alternatively, Mn oxides were incorporated into phospholipid or polyethylene glycol layers in order to increase their biocompatibility and stability in an aqueous medium. Furthermore, Mn(II) complexes have been linked through a suitable linker to inorganic matrices, such as silica nanoparticles. The r_1 values obtained are completely comparable to those observed in the case of the Gd(III) systems. Unlike the Gd-based systems, a notable advantage is the very common occurrence of the fast exchange condition and therefore the absence of a limit to r_1 due to the long lifetime of the coordinated water molecule. However, these nanosystems are generally characterized by a long circulation time before excretion so that issues related to the stability of the complexes or to the possible release of metal ions considerably impact also the development of the nanoprobes. Significant progress in this direction is possible and easily predictable.

In conclusion, studies on Mn(II) compounds as an alternative to current Gd-based MRI CAs are experiencing a rapid and uninterrupted development. The results obtained so far and the new ones that will be available in the coming years will contribute to make available soon a new class of powerful and safe metal-based tools for biomedical research and clinical applications.

Executive Summary:

- The relaxivities of small Mn(II) complexes are generally slightly lower than those of structurally related Gd(III) complexes (~70%), which is mainly a consequence of the lower number of unpaired electrons in high-spin Mn(II) complexes. The scalar mechanism contributes to the relaxivity observed at low fields for Mn(II) complexes only if electronic relaxation is slow and water exchange is not too fast.
- The relaxivities of small Mn(II) complexes can be improved by slowing down their rotational motion in solution (increasing τ_R), so that they overcome those of commercially available Gd(III) contrast agents. Among the different strategies developed to increase τ_R (in both Mn(II) and Gd(III) complexes) are increasing the size of the complex (binuclear, trinuclear…), the formation of micelles, non-covalent binding to proteins or incorporation into nanoparticles.
- Water exchange rates in Mn(II) complexes are generally rather fast, so that slow exchange is not expected to limit ^{1}H relaxivity even for slowly tumbling systems.

- Mn(II)-based systems with promising properties were developed using different strategies including intercalation of discrete chelates in silica and layered materials, inclusion of Mn(II) ions in the inorganic framework of mesoporous silica nanoparticles or preparation of MnO and manganese phosphate nanoparticles.
- The dissociation kinetics profile of Mn(II) complexes with acyclic chelators can be improved by ligand rigidification.
- In spite of the progress achieved during the last decade, developing highly efficient and stable Mn(II)-based contrast agents remains a challenging task.

Figure legends

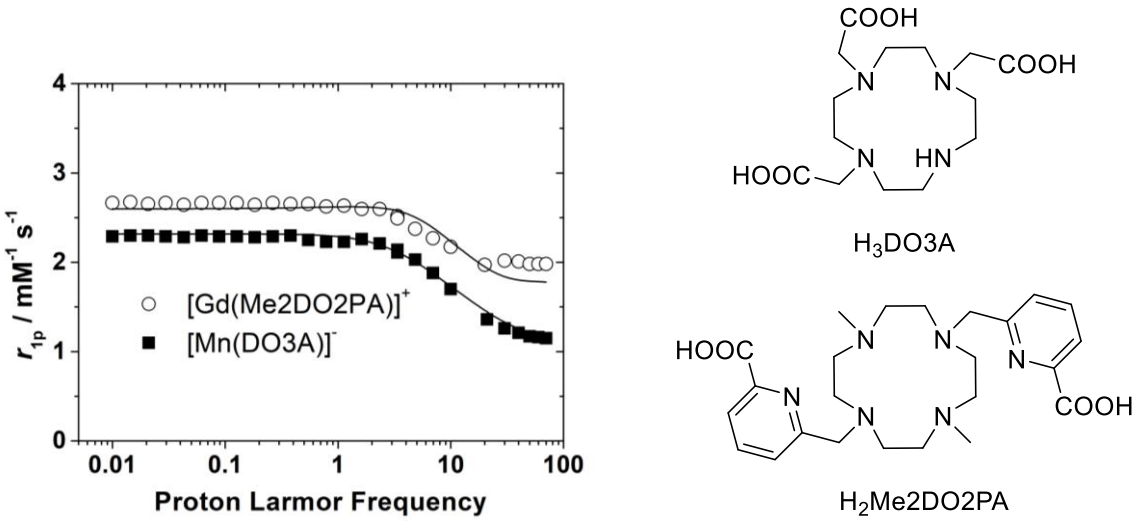

Figure 1. ^{1}H NMRD profiles of [Mn(DO3A)]$^-$ and [Gd(Me2DO2PA)]$^+$ recorded at 25 ºC and the structures of the ligands. The solid lines correspond to the fits of the data as explained in the text.

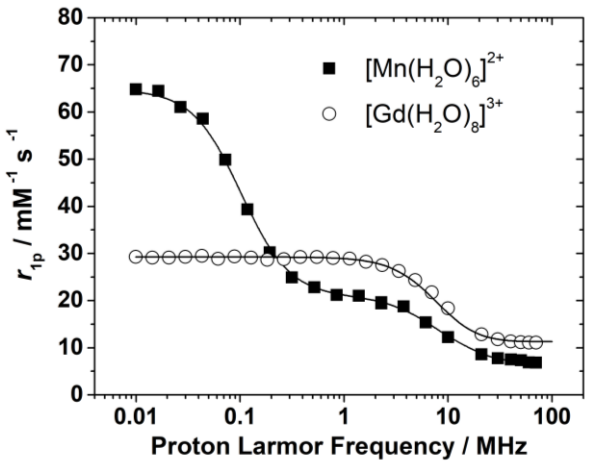

Figure 2. ^{1}H NMRD profiles of $[Mn(H_2O)_6]^{2+}$ and $[Gd(H_2O)_8]^{3+}$ recorded at 25 ºC. The solid lines correspond to the fits of the data as explained in the text.

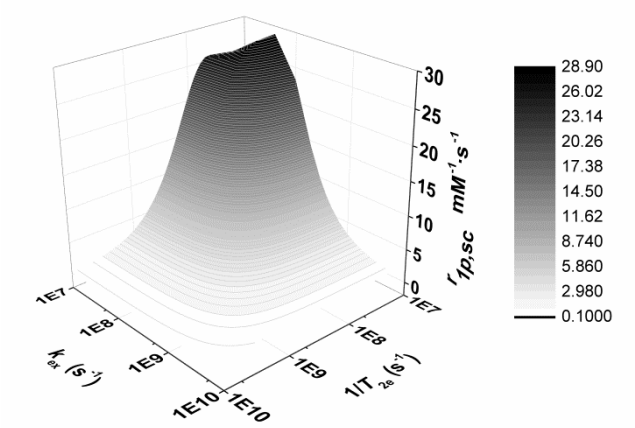

Figure 3. Scalar contribution to the inner-sphere relaxivity calculated for an hypothetical Mn(II) complex as a function of the inverse relaxation time of the electron spin ($1/T_{2e}$) and the exchange rate of the coordinated water molecule ($k_{ex} = 1/\tau_m$). Other parameters are as follows: $A/\hbar$ = 5.43×10^6 rad s^{-1}, q = 1, B = 3×10^{-4} T.

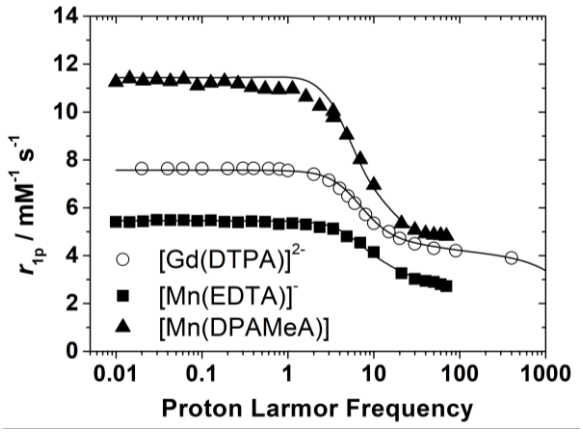

Figure 4. ^{1}H NMRD profiles of [Gd(DTPA)]$^{2-}$, [Mn(DPAMeA)]$^-$ and [Mn(EDTA)]$^-$ recorded at 25 ºC. The solid lines correspond to the fits of the data as explained in the text.

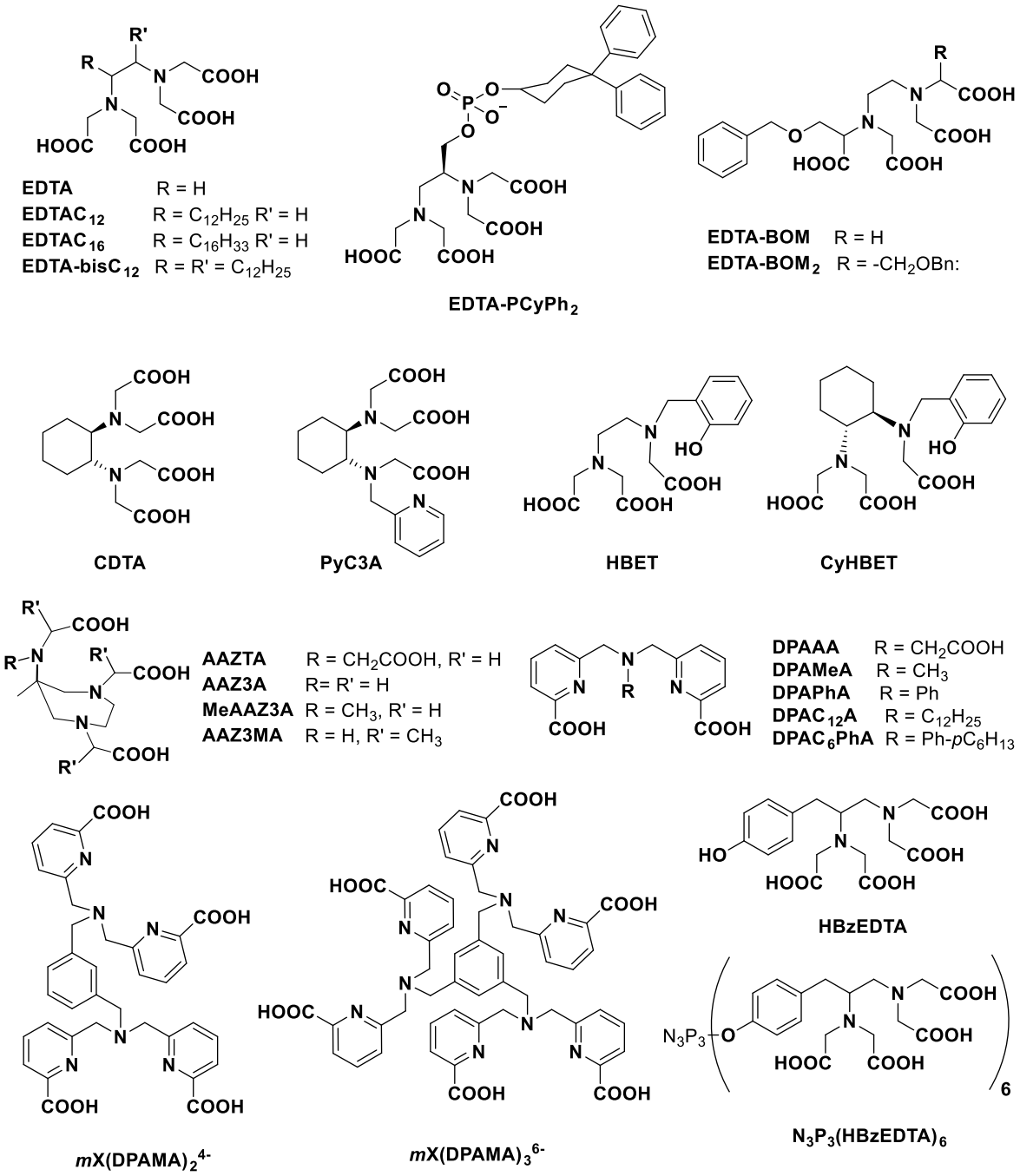

Figure 5. Acyclic ligands discussed in the text.

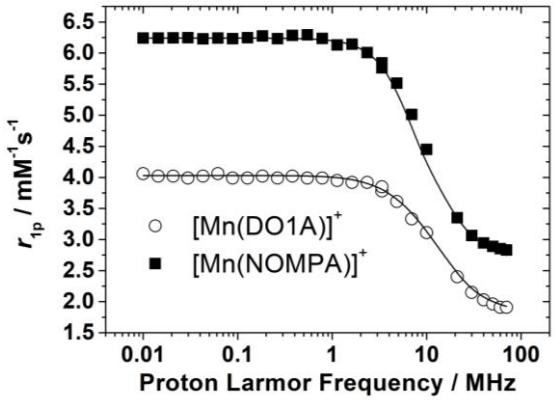

Figure 6. ^{1}H NMRD profiles of $[Mn(DO1A)]^{+}$ and $[Mn(NOMPA)]^{+}$ recorded at 25 ºC. The solid lines correspond to the fits of the data as explained in the text.

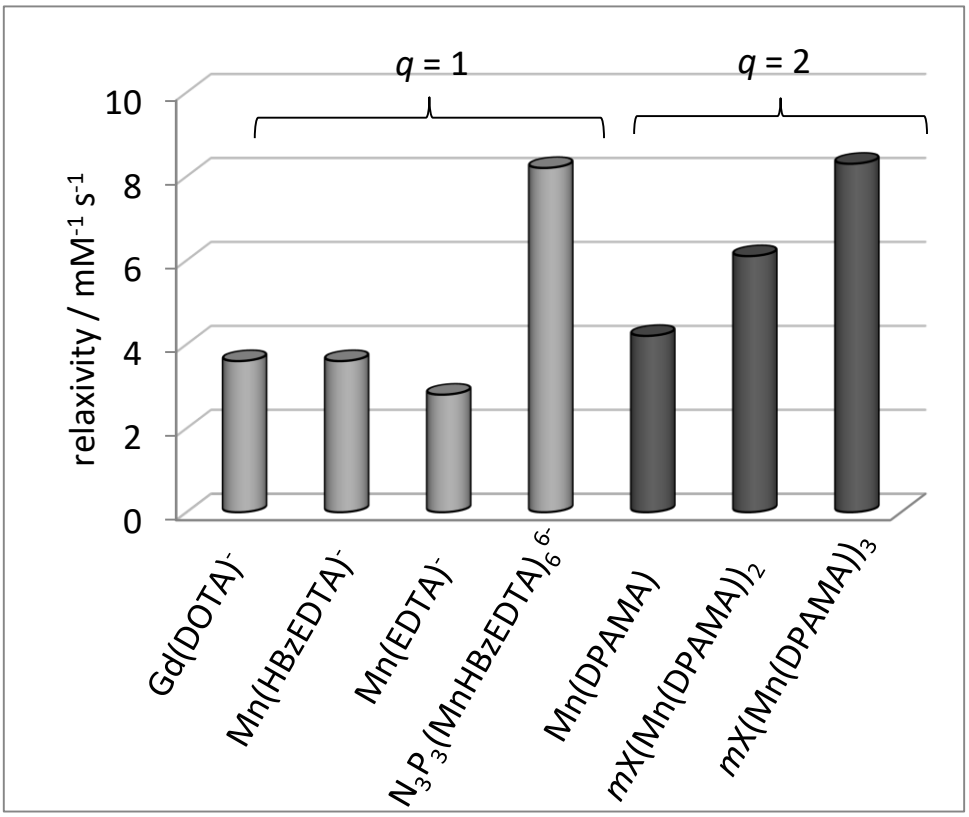

Figure 7. Relaxivities of selected Mn(II) complexes containing one (*q*=1) or two (*q*=2) coordinated water molecules compared to that of $[Gd(DOTA)]^{-}$. All data at 20 MHz and 37 ºC.

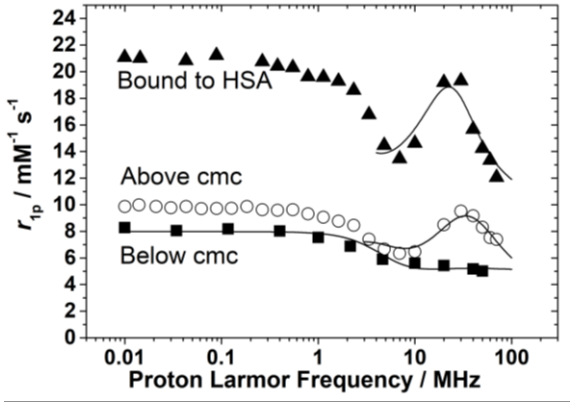

Figure 8. ^{1}H NMRD profiles of [Mn(DPAC12A)] recorded below and above the critical micellar concentration and bound to Human Serum Albumin (HSA). The lines correspond to the fits of the data with the parameters shown in Table 2.

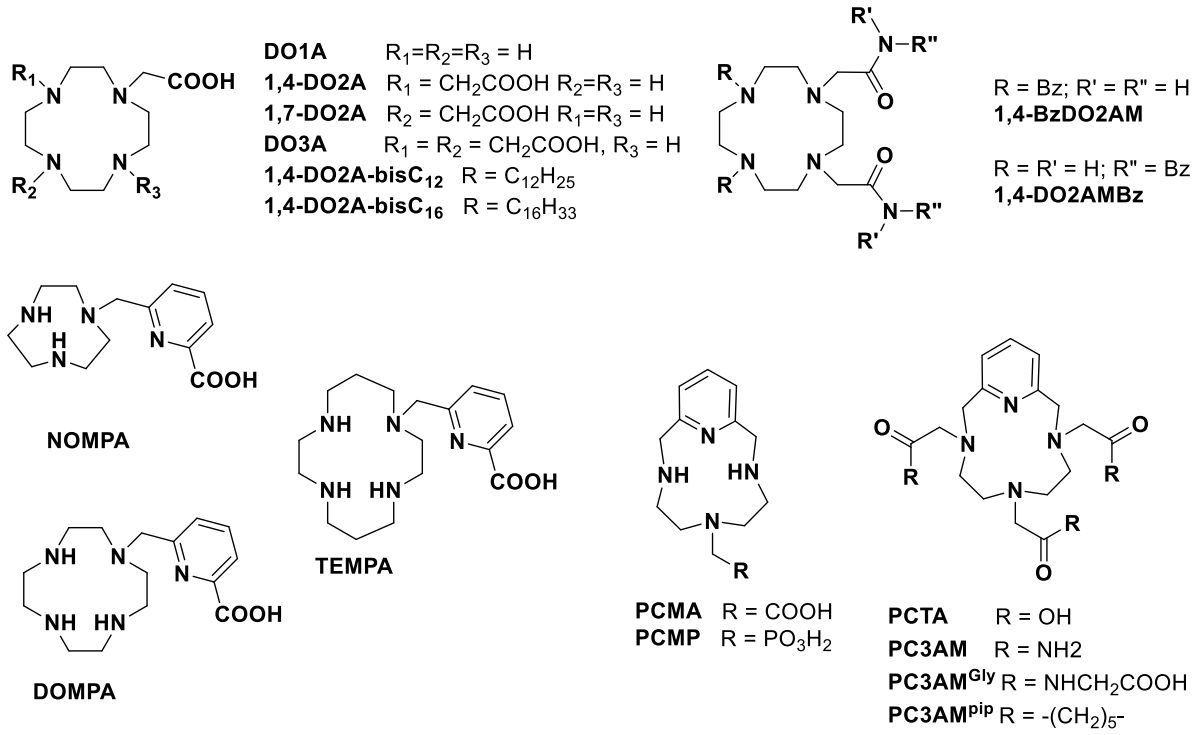

Figure 9. Macrocyclic ligands discussed in the text

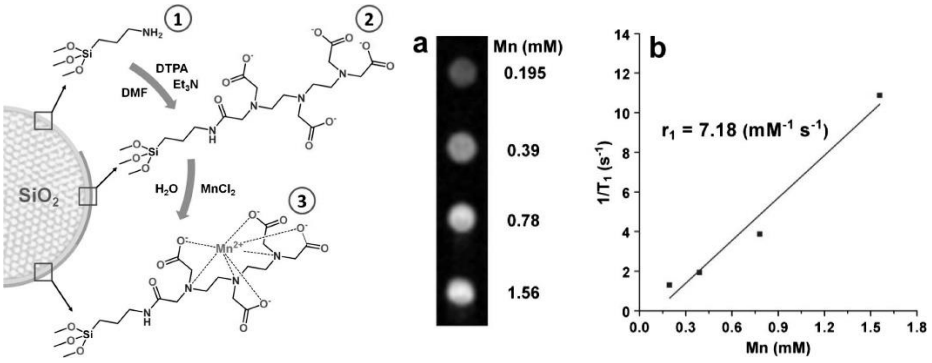

Figure 10. Left: schematic view of the functionalization of the silica nanoparticles with Mn-DTPA chelates; right: T_1-weighted MR image of Mn-DTPA-MSNSs solutions and Plot of $1/T_1$ versus Mn(II) concentration. Adapted from ref. [57]

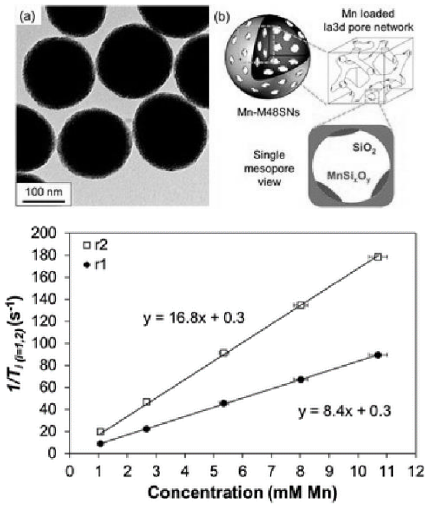

Figure 11. TEM image and schematic representation of the structure of MnSixOy-MSN. Longitudinal (r_1) and transversal (r_2) relaxivities of MnM48SNs at 1.5 T and 37°C. Adapted from ref. [60].

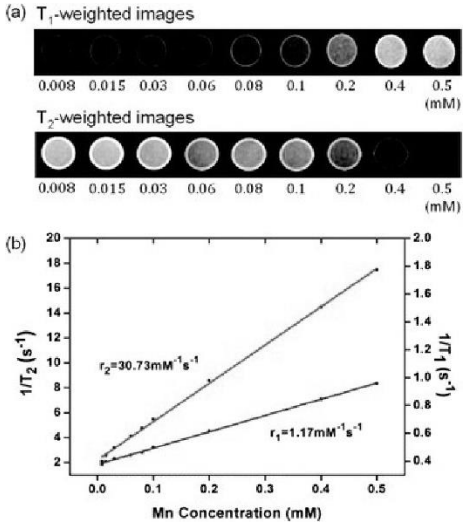

Figure 12. a) T_1- and T_2-weighted MR images of MnO nanoparticles as a function of Mn(II) concentration in aqueous suspension. (b) Plot of $1/T_1$ and $1/T_2$ versus Mn(II) concentration. Adapted from ref. [63]

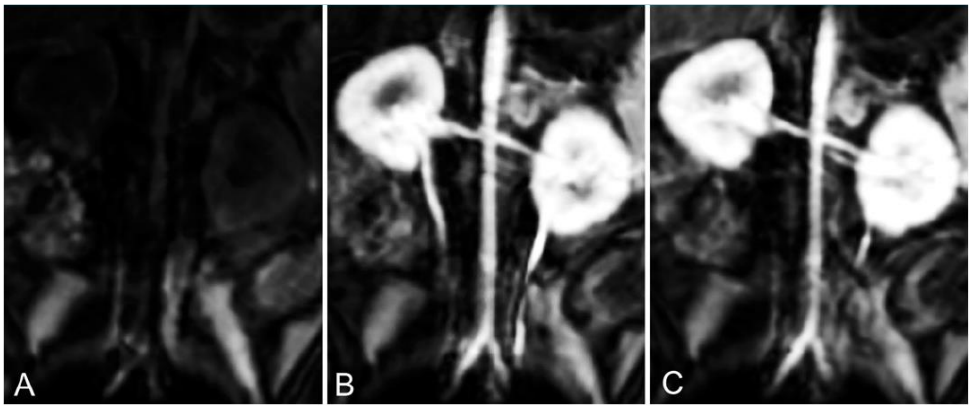

Figure 13. T_1-weighted coronal images acquired at 3.0 T of abdominal aorta and renal arteries, A, prior to injection of contrast agent, B, 9 seconds after injection of 0.1 mmol/kg Mn-PyC3A, and, C, 9 seconds after injection of 0.1 mmol/kg Gd-DTPA. The abdominal aorta versus adjacent muscle CNR was 476 ± 77 for Mn-PyC3A and 538 ± 120 for Gd-DTPA. Adapted from ref. [49].

Table 1. Main parameters governing the relaxivities of different $Mn^{(II)}$ and $Gd^{(III)}$ complexes.

	$[Gd(H_2O)_8]^{3+}$ [a]	$[Mn(H_2O)_6]^{2+}$ [b]	$[Gd(DTPA)(H_2O)]^{2-}$ [a]	$[Mn(EDTA)(H_2O)]^{2-}$ [c]
τ_m^{298}/ ns	2.5	35.5	310	2.1
τ_R^{298} / ps	39	30	66	57
τ_V^{298}/ ps	6.8	10.0	23.8	27.9
D_{MH}^{298} / 10^{-10} m^2 s^{-1}	2.24	23	2.24	23.1
Δ^2 / 10^{19} s^{-2}	8.3	0.06	4.4	6.9
$A_H/\hbar$/ 10^7 rad s^{-1}	[d]	5.43	[d]	[d]
r_{MH}/Å	3.1	2.83	3.0	2.83
a_{MH}/Å	4.0	3.6	4.0	3.6

[a] Obtained by analysis of ^1H NMRD and ^{17}O NMR data, this work. [b] Data from reference.[20] [c] Data from reference.[18] [d] No scalar contribution to relaxivity was observed.

Table 2. Selecterd parameters obtained from the analysis of the NMRD data of [Mn(DPAC12A)] under different conditions.

	Below cmc	Avobe cmc	Bound to HSA
r_{1p} (20 MHz)	5.3	8.5	15.5
τ_{RG} (ns)		5.5	50 (fixed)
τ_{RL} (ps)	123[a]	91	306
S^2		0.27	0.26

[a] Global and local motions not separated.

- **Bibliography:**
- Papers of special note have been highlighted as: *** of interest; ** of considerable interest**

[1] Edelman GM, Hesselink JR, Zlatkin MB, Crues JV. III, Clinical Magnetic Resonance Imaging, Elsevier Health, St. Louis, 3 (2006).

[2] Lohrke J, Frenzel T, Endrikat J, et al. 25 Years of Contrast-Enhanced MRI: Developments, Current Challenges and Future Perspectives. *Adv. Ther.* 33, 1-28 (2016).

[3] https://www.healthsystemtracker.org/chart-collection/how-do-healthcare-prices-and-use-in-the-u-s-compare-to-other-countries/#item-start

[4] Cheng S, Abramova L, Saab G, et al. *J. Am. Med. Assoc.* 297, 1542−1544 (2007).

[5] Di Gregorio E, Ferrauto G, Furlan C, et al. The Issue of Gadolinium Retained in Tissues: Insights on the Role of Metal Complex Stability by Comparing Metal Uptake in Murine Tissues Upon the Concomitant Administration of Lanthanum- and Gadolinium-Diethylentriamminopentaacetate. *Invest. Radiol.* 53, 167–172 (2018).

[6] Pan D, Schmieder AH, Wickline SA, Lanza GM. Manganese-based MRI contrast agents: past, present and future. *Tetrahedron* 67, 8431-8444 (2011).

* **Clear and thorough review on Mn(II)-based contrast agents, with a focus on nanosized agents.**

[7] Rocklage SM, Cacheris WP, Quay SC, Hahn FE, Raymond KN. Syntheses of multidentate ligands containing hydroxypryidyl donor groups. *Inorg. Chem.* 28, 477 (1989).

[8] Crossgrove J, Zheng W. Manganese toxicity upon overexposure. *NMR Biomed.* 17, 544 (2004).

[9] Caravan P, Farrara CT, Frullano L, Uppal R. Influence of molecular parameters and increasing magnetic field strength on relaxivity of gadolinium- and manganese-based T_1 contrast agents. *Contrast Media Mol. Imaging.* 4, 89–100 (2009).

** **Excellent and comprehensive discussion of the relaxometry properties of Mn(II) contrast agents.**

[10] Drahos B, Lukes I, Toth E. Manganese(II) Complexes as Potential Contrast Agents for MRI. *Eur. J. Inorg. Chem.* 1975 (2012).

** **Comprehensive reviews of Mn(II)-based systems updated to 2011.**

[11] Kueny-Stotz M, Garofalo A, Felder- Flesch D. Manganese-Enhanced MRI Contrast Agents: From Small Chelates to Nanosized Hybrids. *Eur. J. Inorg. Chem.* 1987 (2012).

** **Comprehensive reviews of Mn(II)-based systems updated to 2011.**

[12] Kim WD, Kiefer GE, Maton F, McMillan K, Muller RN, Sherry, AD. Relaxometry, Luminescence Measurements, Electrophoresis, and Animal Biodistribution of Lanthanide(III) Complexes of Some Polyaza Macrocyclic Acetates Containing Pyridine. *Inorg. Chem.* 34, 2233−2243 (1995).

[13] Delli Castelli D, Gianolio E, Aime S. MRI Contrast Agents: State of the Art and New Trends, Ch 8 of Bioinorganic Medicinal Chemistry. Ed. Alessio E, Weinheim: WILEY-VCH (2011).

[14] Freed, JH. Dynamic effects of pair correlation functions on spin relaxation by translational diffusion in liquids. II. Finite jumps and independent T_1 processes. *J. Chem. Phys.* 68, 4034−4037 (1978).

[15] McLachlan, AD. Line Widths of Electron Resonance Spectra in Solution. *Proc. R. Soc. London.* A280, 271−288 (1964).

[16] Solomon I, Bloembergen M. Nuclear Magnetic Interactions in the HF Molecule. *J. Chem. Phys.* 25, 261−266 (1956).

[17] Bloembergen N, Morgan LO. Proton Relaxation Times in Paramagnetic Solutions. Effects of Electron Spin Relaxation. *J. Chem. Phys.* 34, 842−850 (1961).

[18] Rolla GA, Platas Iglesias C, Botta M, Tei L, Helm L. ^{1}H and ^{17}O NMR relaxometric and computational study on macrocyclic Mn(II) complexes. *Inorg. Chem.* 52, 3268-3279 (2013).

* **Detailed analysis of structure vs relaxivity relationship on a series of cyclen-based Mn(II) complexes.**

[19] Rodríguez-Rodríguez A, Esteban-Gomez D, de Blas A, et al. Lanthanide(III) Complexes with Ligands Derived from a Cyclen Framework Containing Pyridinecarboxylate Pendants. The Effect of Steric Hindrance on the Hydration Number. *Inorg. Chem.* 51, 2509−2521 (2012).

* **Detailed analysis of structure vs relaxivity relationship on a series of cyclen-based Mn(II) complexes.**

[20] Esteban-Gómez D, Cassino C, Botta M, Platas-Iglesias C. ^{17}O and ^{1}H Relaxometric and DFT Study of Hyperfine Coupling Constants in $[Mn(H_2O)_6]^{2+}$. *RSC Adv.* 4, 7094−7103 (2014).

[21] Powell DH, Ni Dhubhghaill OM, Pubanz D, et al. Structural and Dynamic Parameters Obtained from ^{17}O NMR, EPR, and NMRD Studies of Monomeric and Dimeric $Gd^{(III)}$ Complexes of Interest in Magnetic Resonance Imaging: An Integrated and Theoretically Self-Consistent Approach. *J. Am. Chem. Soc.* 118, 9333−9346 (1996).

[22] Astashkin AV, Raitsimring AM, Caravan P. Pulsed ENDOR Study of Water Coordination to Gd^{III} Complexes in Orientationally Disordered Sytems. *J. Phys Chem. A.* 108, 1990−2001 (2004).

[23] Aime S, Calabi L, Cavallotti C, et al. [GdAAZTA]: A New Structural Entry for an Improved Generation of MRI Contrast Agents. *Inorg. Chem.* 43, 7588−7590 (2004).

[24] Botta M, Aime S, Barge A, et al. Ternary Complexes between Cationic Gd^{III} Chelates and Anionic Metabolites in Aqueous Solution: An NMR Relaxometric Study. *Chem. Eur. J.* 9, 2102−2109 (2004).

[25] Regueiro-Figueroa M, Rolla GA, Esteban-Gómez D, et al. High relaxivity Mn^{II}-based MRI contrast agents. *Chem. Eur. J.* 52, 17300–17305 (2014).

[26] Gale EM, Zhu J, Caravan P. Direct Measurement of the Mn(II) Hydration State in Metal Complexes and Metalloproteins through ^{17}O Linewidths. *J. Am. Chem. Soc.* 135, 18600−18608 (2013).

[27] Peters JA, Geraldes CFGC. A Semi-Empirical Method for the Estimation of the Hydration Number of Mn(II)-Complexes. *Inorganics* 6, 116 (2018).

[28] Molnár E, Camus N, Patinec V, et al. Picolinate-containing macrocyclic Mn^{II} complexes as potential MRI contrast agents. *Inorg. Chem.* 53, 5136−5149 (2014).

[29] Forgacs A, Regueiro-Figueroa M, Barriada JL, et al. Mono , Bi , and Trinuclear Bis-Hydrated Mn^{II} Complexes as Potential MRI Contrast Agents. *Inorg. Chem.* 54, 9576−9587 (2015).

[30] Zhu J, Gale EM, Atanasova IP, Rietz TA, Caravan P. Hexameric Mn^{II} Dendrimer as MRI Contrast Agent. *Chem. Eur. J.* 20, 14507 – 14513 (2014).

* **A multimeric- high relaxivity Mn(II)-based contrast agent**

[31] Rolla GA, De Biasio V, Giovenzana GB, Botta M, Tei L. Supramolecular assemblies based on amphiphilic Mn^{II}-complexes as high relaxivity MRI probes. *Dalton Trans.* 47, 10660-10670 (2018).

* **A series of EDTA- and 1,4-DO2A-based amphiphilic Mn(II) complexes forming macromolecular adducts of high relaxivity.**

[32] Forgács A, Tei L, Baranyai Z, Esteban-Gómez D, Platas-Iglesias C, Botta M. Optimising the relaxivities of $Mn^{(II}$ complexes by targeting human serum albumin (HSA). *Dalton Trans.* 6, 8494-8504 (2017).

[33] Forgács A, Pujales-Paradela R, Regueiro-Figueroa M, et al. Developing the family of picolinate ligands for Mn^{II} complexation. *Dalton Trans.* 46, 1546–1558 (2017).

[34] Lipari G, Szabo A, Model-free approach to the interpretation of nuclear magnetic resonance relaxation in macromolecules. 1. Theory and range of validity. *J. Am. Chem. Soc.* 104, 4546-4559 (1982).

[35] G. Lipari, A. Szabo, Model-free approach to the interpretation of nuclear magnetic resonance relaxation in macromolecules. 2. Analysis of experimental results. *J. Am. Chem. Soc.* 104, 4559-4570 (1982).

[36] Pujales-Paradela R, Regueiro-Figueroa M, Esteban-Gomez D, Platas-Iglesias C, Transition Metal-based T_1 Contrast Agents, Ch 5 of Contrast Agents for MRI. Experimental Methods. Eds. Pierre VC, Allen MJ, Croydon: The Royal Society of Chemistry (2018).

[37] Forgács A, Tei L, Baranyai Z, Tóth I, Zékány L, Botta M. Bisamide Derivative of [Mn(1,4-DO2A)]: Solution Thermodynamic, Kinetic and NMR Relaxometric Studies. *Eur. J. Inorg. Chem.* 1165–1174 (2016).

[38] Gale EM, Atanasova IP, Blasi F, Ay I, Caravan P. Manganese Alternative to Gadolinium for MRI Contrast. *J. Am. Chem. Soc.* 137, 15548−15557 (2015).

** **Mn(PyC3A): from the synthesis to the stability and in vivo application of a new promising MRI probe.**

[39] Drahos B, Kotek J, Cisarova I, et al. Mn^{II} Complexes with 12-membered Pyridine Based Macrocycles Bearing Carboxylate or Phosphonate Pendant Arm: Crystallographic, Thermodynamic, Kinetic, Redox, and $^{1}H/^{17}O$ Relaxation Studies. *Inorg. Chem.* 50, 12785–12801 (2011).

[40] Manganese and its role in biological processes, vol. 37 of the series "METAL IONS IN BIOLOGICAL SYSTEMS" edited by A Sigel and H Sigel, Marcel Dekker Inc., New York (2000).

[41] Crossgrove J, Zheng W. Manganese toxicity upon overexposure. *NMR Biomed.* 17, 544–553 (2004).

[42] O'Neal SL, Zheng W. Manganese toxicity upon overexposure: a decade in review. *Curr Environ Health Rep.* 2(3), 315–328 (2015).

[43] Brücher E, Tircsó G, Baranyai Z, Kovács Z, Sherry Ad. Stability and Toxicity of Contrast Agents, Ch 4 of The Chemistry of Contrast Agents in Medical Magnetic Resonance Imaging, 2nd Edn. Eds. Merbach AE, Helm L, Tóth É, New York, NY: John Wiley & Sons (2013).

[44] Kálmán FK, Tircsó G. Kinetic inertness of the Mn(II) complexes formed with AAZTA and some open-chain EDTA derivatives. *Inorg. Chem.* 51, 10065−10067 (2012).

[45] Aime S, Anelli PL, Botta M, et al. Relaxometric evaluation of novel manganese(II) complexes for application as contrast agents in magnetic resonance imaging. *J. Biol. Inorg. Chem.* 7, 58–67 (2002).

[46] Troughton JS, Greenfield MT, Greenwood JM, et al. Synthesis and Evaluation of a High Relaxivity Manganese(II)-Based MRI Contrast Agent. *Inorg. Chem.* 43, 6313–6323 (2004).

[47] Baroni S, Colombo Serra S, Fringuello Mingo A, Lux G, Giovenzana GB, Lattuada L. Synthesis and Relaxometric Characterization of a New Mn(II)-EDTA-Deoxycholic Acid Conjugate Complex as a Potential MRI Blood Pool Agent. *Chem. Select.* 1, 1607–1612 (2016).

[48] Molnár E, Váradi B, Garda Z, et al. Remarkable differences and similarities between the isomeric Mn(II)-cis and trans-1,2-diaminocyclohexane-N,N,N',N'-tetraacetate complexes. *Inorg. Chim. Acta.* 472, 254–263 (2018).

[49] Gale EM, Wey HY, Ramsay I, Yen YF, Sosnovik DE, Caravan P. A manganese-based alternative to gadolinium: contrast-enhanced MR angiography, excretion, pharmacokinetics, and metabolism. *Radiology* 286(3), 865-872 (2018).

[50] Loving GS, Mukherjee S, Caravan P. Redox-Activated Manganese-Based MR Contrast Agent. *J. Am. Chem. Soc.* 135, 4620−4623 (2013).

[51] Gale EM, Mukherjee S, Liu C, Galen S. Loving GS, Caravan P. Structure−redox−relaxivity relationships for redox responsive Manganese-based Magnetic Resonance Imaging probes. *Inorg. Chem.* 53, 10748−10761 (2014).

[52] Tei L, Gugliotta G, Fekete M, Kalman FK, Botta M. Mn(II) complexes of novel hexadentate AAZTA-like chelators: a solution thermodynamics and relaxometric study. *Dalton Trans.* 40, 2025-2032 (2011).

[53] Garda Z, Molnár E, Kálmán FK, et al. Effect of the nature of donor atoms on the thermodynamic, kinetic and relaxation properties of Mn(II) complexes formed with some trisubstituted 12-membered macrocyclic ligands. *Front. Chem.* 6, 232 (2018).

[54] Garda Z, Forgacs A, Do QN, et al. Physico-chemical properties of Mn^{II} complexes formed with cis- and trans-DO2A: thermodynamic, electrochemical and kinetic studies. *J. Inorg. Biochem.* 163, 206-213 (2016).

[55] Botta M, Tei L. Relaxivity Enhancement in Macromolecular and Nanosized GdIII-Based MRI Contrast Agents *Eur. J. Inorg. Chem.* 1945-1960 (2012).

[56] Carniato F, Tei L, Botta M. Gd-based Mesoporous Silica Nanoparticles as MRI Probes. *Eur. J. Inorg. Chem.* 4936–4954 (2018).

[57] Pálmai M, Pethő A, Naszályi Nagy L, et al. Direct immobilization of manganese chelates on silica nanospheres for MRI applications. *Journal of Colloid and Interface Science.* 498, 298–305 (2017).

[58] Jin M, Li W, Spillane DEM, Geraldes CFGC, Williams GR, Annie Bligh SW. Hydroxy double salts intercalated with Mn(II) complexes as potential contrast agents. *Solid State Sciences.* 53, 9-16 (2016).

[59] Chen Y, Chen H, Zhang S, et al. Structure-property relationships in manganese oxide--mesoporous silica nanoparticles used for T_1-weighted MRI and simultaneous anti-cancer drug delivery. *Biomaterials.* 33, 2388-2398 (2012).

[60] Guillet-Nicolas R, Laprise-Pelletier M, Nair MM, et al. Manganese-impregnated mesoporous silica nanoparticles for signal enhancement in MRI cell labelling studies. *Nanoscale.* 5, 11499-11511 (2013).

[61] Niu D, Luo X, Li Y, Liu X, Wang X, Shi J. Manganese-Loaded Dual-Mesoporous Silica Spheres for Efficient T_1- and T_2-Weighted Dual Mode Magnetic Resonance Imaging. *ACS Appl. Mater. Interfaces.* 5, 9942−9948 (2013).

[62] Hsu BYW, Kirby G, Tan A, Seifalian AM, Li X, Wang J. Relaxivity and toxicological properties of manganese oxide nanoparticles for MRI applications. *RSC Adv.* 6, 45462-45474 (2016).

* **Review of Mn-oxide nanoparticles for MRI applications, with a focus on their relaxivity and toxicological properties.**

[63] Hsu BYW, Wang M, Zhang Y, et al. Silica–F127 nanohybrid-encapsulated manganese oxide nanoparticles for optimized T_1 magnetic resonance relaxivity. *Nanoscale.* 6, 293-299 (2014).

[64] Bañobre-López M, García-Hevia L, Cerqueira MF, Rivadulla F, Gallo J. Tunable Performance of Manganese Oxide Nanostructures as MRI Contrast Agents. *Chem. Eur. J.* 24, 1295-1303 (2018).

[65] Gao H, Liu X, Tang W, et al. ^{99m}Tc-conjugated manganese-based mesoporous silica nanoparticles for SPECT, pH-responsive MRI and anti-cancer drug delivery. *Nanoscale.* 8, 19573-19580 (2016).

[66] Hao Y, Zheng C, Wang L, et al. Tumor acidity-activatable manganese phosphate nanoplatform for amplification of photodynamic cancer therapy and magnetic resonance imaging. *Acta Biomaterialia.* 62, 293–305 (2017).

[67] Hamm B, Vogl TJ, Branding G, et al. Focal liver lesions: MR imaging with Mn-DPDP--initial clinical results in 40 patients. *Radiology*. 182, 167-174 (1992).

[68] Ni Y, Petré C, Bosmans H, et al. Comparison of manganese biodistribution and MR contrast enhancement in rats after intravenous injection of MnDPDP and $MnCl_2$. *Acta Radiol.* 38, 700-707 (1997).

[69] Gale EM, Caravan P. Gadolinium-free contrast agents for Magnetic Resonance Imaging of the Central Nervous System. *ACS Chem. Neurosci.* 9, 395−397 (2018).

[70] Wang J, Wang H, Ramsay IA, et al. Manganese-Based Contrast Agents for Magnetic Resonance Imaging of Liver Tumors: Structure−Activity Relationships and Lead Candidate Evaluation. *J. Med. Chem.* 61, 8811−8824 (2018).

[71] Islam K, Kim S, Kim HK, et al. Manganese complex of ethylenediaminetetraacetic Acid (EDTA)–benzothiazole aniline (BTA) conjugate as a potential liver-targeting MRI contrast agent. *J. Med. Chem.* 60, 7, 2993-3001 (2017).

[72] Pan D, Caruthers SD, Senpan A, Schmieder AH, Wickline SA, Lanza GM. Revisiting an old friend: manganese-based MRI contrast agents. *WIREs Nanomed. Nanobiotech.* 3, 162-173 (2011).

[73] Fischer HC, Chan WCW. Nanotoxicity: the growing need for in vivo study. *Curr. Opin. Biotech.* 18, 565–571 (2007).

[74] Dobrovolskaia MA, Germolec DR, Weaver JL, Evaluation of nanoparticle immunotoxicity. *Nat. Nanotechnol.* 4, 411–414 (2009).

[75] Xiao J, X. Tian XM, Yang C, et al. Ultrahigh relaxivity and safe probes of manganese oxide nanoparticles for in vivo imaging. *Sci. Rep.* 3, 3424 (2013).

[76] Li JJ, Wu C, Hou PF, Zhang M, Xu K. One-pot preparation of hydrophilic manganese oxide nanoparticles as T-1 nano-contrast agent for molecular magnetic resonance imaging of renal carcinoma in vitro and in vivo. *Biosens. Bioelectron.* 102, 1-8 (2018).

[77] The Chemistry of Contrast Agents in Medical Magnetic Resonance Imaging, 2nd Edn. Eds. Merbach AE, Helm L, Tóth É, New York, NY: John Wiley & Sons (2013)

[78] Contrast Agents for MRI. Experimental Methods. Eds. Pierre VC, Allen MJ, Croydon: The Royal Society of Chemistry (2018).